Since January 2020 Elsevier has created a COVID-19 resource centre with free information in English and Mandarin on the novel coronavirus COVID-19. The COVID-19 resource centre is hosted on Elsevier Connect, the company's public news and information website.

Cell Reports

Article

BRD4 Prevents R-Loop Formation and Transcription-Replication Conflicts by Ensuring Efficient Transcription Elongation

Graphical Abstract

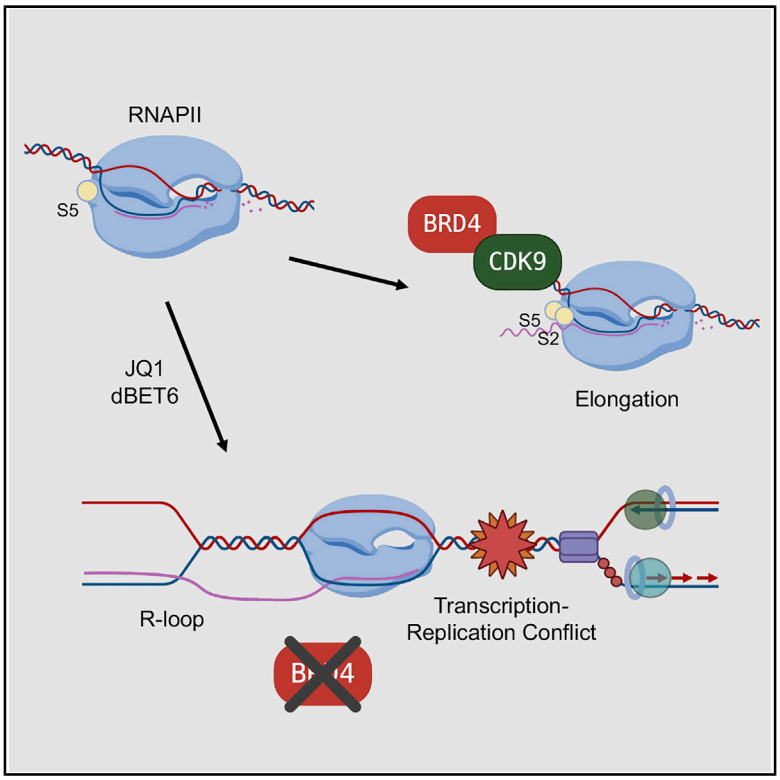

Authors

Drake S. Edwards, Rohin Maganti, Jarred P. Tanksley, ..., Elena Balkanska-Sinclair, Jinjie Ling, Scott R. Floyd

Correspondence

scott.floyd@duke.edu

In Brief

BRD4 plays a known role in transcription activation through an interaction with CDK9. Edwards et al. show that BET inhibitors and degraders have cytotoxic effects through the formation of R-loops, causing transcription-replication conflicts, DNA damage, and cell death.

Highlights

- BET protein LOF leads to an increase in DNA damage
- BET LOF damage is dependent on S-phase and chromatin occupation of RNAPII
- BRD4 overexpression rescues BET LOF and requires CDK9 interaction domain
- BET protein LOF damage is correlated with R-loop formation

Edwards et al., 2020, Cell Reports *32*, 108166
September 22, 2020
https://doi.org/10.1016/j.celrep.2020.108166

CellPress

Cell Reports

CellPress
OPEN ACCESS

Article

BRD4 Prevents R-Loop Formation and Transcription-Replication Conflicts by Ensuring Efficient Transcription Elongation

Drake S. Edwards,[1,2,3] Rohin Maganti,[4] Jarred P. Tanksley,[3] Jie Luo,[3] James J.H. Park,[3] Elena Balkanska-Sinclair,[3] Jinjie Ling,[4] and Scott R. Floyd[2,3,5,*]

[1]Medical Scientist Training Program, Duke University School of Medicine, Durham, NC 27710, USA
[2]Department of Pharmacology and Cancer Biology, Duke University School of Medicine, Durham, NC 27710, USA
[3]Department of Radiation Oncology, Duke University School of Medicine, Durham, NC 27710, USA
[4]Duke University, Durham, NC 27710, USA
[5]Lead Contact
*Correspondence: scott.floyd@duke.edu
https://doi.org/10.1016/j.celrep.2020.108166

SUMMARY

Effective spatio-temporal control of transcription and replication during S-phase is paramount to maintaining genomic integrity and cell survival. Dysregulation of these systems can lead to conflicts between the transcription and replication machinery, causing DNA damage and cell death. BRD4 allows efficient transcriptional elongation by stimulating phosphorylation of RNA polymerase II (RNAPII). We report that bromodomain and extra-terminal domain (BET) protein loss of function (LOF) causes RNAPII pausing on the chromatin and DNA damage affecting cells in S-phase. This persistent RNAPII-dependent pausing leads to an accumulation of RNA:DNA hybrids (R-loops) at sites of BRD4 occupancy, leading to transcription-replication conflicts (TRCs), DNA damage, and cell death. Finally, our data show that the BRD4 C-terminal domain, which interacts with P-TEFb, is required to prevent R-loop formation and DNA damage caused by BET protein LOF.

INTRODUCTION

Maintaining the integrity of the genome throughout the cell cycle is paramount to cell survival (Hanahan and Weinberg, 2011); therefore, complex systems have evolved to tackle various threats to the genome's integrity (Blackford and Jackson, 2017; Cimprich and Cortez, 2008; Hamperl and Cimprich, 2016). During S-phase, areas of chromatin that are engaged in generating RNA transcripts must be coordinated with migrating replication forks. Disruption of either transcription or replication control and coordination can lead to the desynchronization of these chromatin-based activities, resulting in transcription-replication conflicts (TRCs) and subsequent replication stress, DNA damage, and cell death (Aguilera and Gómez-González, 2017; Gaillard and Aguilera, 2016; García-Muse and Aguilera, 2016; El Hage et al., 2010; Sollier and Cimprich, 2015). To avoid these collisions, these processes are separated in both time and space through the activity of several known chromatin-based complexes (Hamperl and Cimprich, 2016). Specifically, the processivity of both the replication machinery and the nascent RNA strand are critical to preventing collisions between the two (Schwab et al., 2015; Zeman and Cimprich, 2014). These systems are an active area of study, especially in cancer cells, as many amplified transcription programs and more frequent replication distinguish cancer cells from normal cells (Kotsantis et al., 2016; Stork et al., 2016). The strategies that cancer cells employ to avoid TRCs are therefore of potential therapeutic interest, as the components of these TRC-avoidance mechanisms could be targeted with a wide therapeutic window in a variety of cancers.

One source of TRCs is the aberrant formation of RNA:DNA hybrids (R-loops), caused by nascent RNA re-annealing with its DNA template strand, forming a three-stranded structure (Aguilera and Gómez-González, 2017; Costantino and Koshland, 2018; Crossley et al., 2019; García-Muse and Aguilera, 2019; Hamperl and Cimprich, 2016; Hamperl et al., 2017; Richard and Manley, 2017; Santos-Pereira and Aguilera, 2015; Sollier and Cimprich, 2015). R-loops play various physiological roles, including immunoglobulin (Ig) class-switching, CRISPR-Cas9 bacterial defense systems, and normal transcription regulation (Chaudhuri and Alt, 2004; García-Muse and Aguilera, 2019; Shao and Zeitlinger, 2017; Skourti-Stathaki and Proudfoot, 2014; Stuckey et al., 2015; Xiao et al., 2017). However, pathologic R-loops can also form from dysregulated transcription, and these pathologic R-loops can impede the progression of the transcription bubble (Crossley et al., 2019). In the case where RNA polymerase II (RNAPII) is stalled, the nascent RNA is allowed to re-anneal with its template strand and form a stable R-loop, leading to the tethering of RNAPII to the chromatin. During S-phase, these R-loop-tethered transcription bubbles create a roadblock for replication forks (Gan et al., 2011; Matos et al., 2019). If these roadblocks are not resolved, collisions with the

replication machinery will lead to replication fork breakdown and DNA strand breaks. Important factors have been identified that prevent and resolve R-loops, including the RNAPII activator CDK9 and the RNA:DNA hybrid endonuclease RNase H1 (Chen et al., 2017; Grunseich et al., 2018; Matos et al., 2019; Morales et al., 2016; Nguyen et al., 2017; Parajuli et al., 2017; Shivji et al., 2018; Skourti-Stathaki et al., 2011; Wahba et al., 2011; Wessel et al., 2019; Zatreanu et al., 2019).

BRD4, a member of the bromodomain and extra-terminal domain (BET) protein family, is a known regulator of transcription elongation. Through its C-terminal domain (CTD) it is known to activate CDK9, the RNAPII-phosphorylating component of the positive transcription elongation factor, P-TEFb (Chen et al., 2014; Itzen et al., 2014; Jang et al., 2005; Kanno et al., 2014; Liu et al., 2013; Patel et al., 2013; Rahman et al., 2011; Winter et al., 2017; Zhang et al., 2012). After RNAPII has initiated transcription and paused, at many genomic loci, BRD4 releases P-TEFb from its inhibitory complex and allows CDK9 to phosphorylate the second serine of the YSPTSPS repeat on the tail of RNAPII (RNAPIIpS2). Once this phosphorylation event occurs, RNAPII is able to enter the elongation phase of transcription. Consequently, inhibition of BRD4 function reduces the transcription of many genes (Delmore et al., 2011; Filippakopoulos et al., 2010; Muhar et al., 2018; Winter et al., 2017).

BET family inhibitors have shown activity in pre-clinical models of several cancers, and clinical trials have shown some efficacy, yet mechanisms of action and predictive biomarkers remain elusive. Recently, members of the BET-bromodomain family have been implicated in both replication stress and R-loop biology (Bowry et al., 2018; Kim et al., 2019; Wessel et al., 2019). In an effort to illuminate the role BRD4 plays in preventing cancer cell death, we studied how DNA damage repair systems react to BET inhibition. We see that BET inhibitors cause double-strand breaks in cells undergoing S-phase replication. Furthermore, we see that overexpression of long-isoform BRD4 (BRD4L, Isoform A) rescues the effects of BRD4 loss, but rescue fails when BRD4 is truncated to delete the P-TEFb-interacting CTD. Finally, we see that BET inhibitors cause an RNAPII-dependent increase in the formation of R-loops, and overexpression of RNase H1, an endonuclease that acts on the RNA strand of R-loops, reverses BET-inhibitor-induced DNA damage. These data suggest a new role for BRD4 in preventing aberrant R-loop formation and TRCs by ensuring efficient RNAPII transcription.

RESULTS

Inhibition or Degradation of BET Family Proteins Leads to Spontaneous DNA Damage in Cancer Cells

BRD4, through its two N-terminal bromodomains, interacts with chromatin by binding to acetylated histones (Filippakopoulos et al., 2012). In previous work, we have described how a low-abundance isoform of BRD4 (Isoform B) mediated chromatin dynamics and DNA damage signaling triggered by ionizing radiation (Floyd et al., 2013). However, small-molecule BET-bromodomain protein inhibitors are effective against cancer cells in the absence of radiation (Asangani et al., 2014; Dawson et al., 2011; Rathert et al., 2015; Zuber et al., 2011). Several groups have reported variable effects of BET-bromodomain inhibitors on DNA damage signaling (Bowry et al., 2018; Floyd et al., 2013; Kim et al., 2019; Pericole et al., 2019; Schröder et al., 2012; Sun et al., 2018; Zhang et al., 2018). We therefore sought to understand the DNA damage consequences of BET-bromodomain inhibition in the absence of exogenous genotoxic sources. JQ1, a small-molecule inhibitor of BET family proteins, binds to the bromodomains and competitively prevents BRD4 from interacting with chromatin (Filippakopoulos et al., 2010). In order to test whether JQ1 was able to induce a DNA damage response, we treated HeLa, HCT-116, and OCI-AML2 cells with (500 nM) JQ1 and stained for γH2AX foci, a marker of DNA damage (Rogakou et al., 1998). We observed that JQ1 was able to induce γH2AX foci formation, indicating that chromatin-bound BET proteins can prevent spontaneous DNA damage (Figures 1A, 1B, and S1A–S1C). We also tested JQ1 effects on normal cells and cells expressing oncogenic drivers. Normal mouse embryonic fibroblasts (MEFs) showed no DNA damage response to JQ1, while MEFs expressing mutant Kras showed a robust γH2AX response after JQ1 exposure (Figure S2C).

Building on small-molecule bromodomain inhibitors, proteolysis targeting chimera (PROTAC) small molecules have been designed to cause potent and rapid degradation of BET proteins (Lu et al., 2015; Winter et al., 2017). These PROTAC molecules link the target protein to an E3-ligase recruiter that causes ubiquitination and subsequent rapid degradation, enabling visualization of BET protein loss and more potent BET protein inhibition with rapid kinetics. We observed that the BET-bromodomain-directed PROTAC dBET6 elicited a robust DNA damage response, detectable by western blot in HeLa cells at 100-nM concentration in as few as 6 h. Concurrent with dBET6-induced loss of BET proteins, we observed a reduction in RNAPII phospho-Serine 2 and saw γH2AX signaling by both western blot and immunofluorescence (Figures 1C–1E). These observations confirmed that loss of BET proteins can result in increased DNA damage signaling. In addition to JQ1 and dBET6, other small molecules that have been used in clinical trials or that target a specific bromodomain led to an increase in γH2AX signaling in HeLa and OCI-AML2 cells at clinically relevant doses (Faivre et al., 2020; Odore et al., 2016; Ozer et al., 2018) (Figures 1H and S1C).

While γH2AX is a general marker for DNA damage signaling, we sought to establish whether BET protein loss also leads to an increase in physical DNA damage such as double-strand breaks. Therefore, we employed single-cell electrophoresis (neutral comet assay) to measure the number of DNA double-strand breaks after dBET6 treatment. Interestingly, we found that in addition to the DNA damage signaling increase, dBET6 increased the number of DNA double-strand breaks (Figures 1F and 1G). These observations indicate that loss of the BET family of proteins can cause physical DNA damage as well as a robust DNA damage response.

BET Protein Loss Induces DNA Damage during S-Phase

TRCs, by definition, occur while the cell is actively replicating its genome during S-phase. An active replication fork, when it collides with a transcription bubble in the head-on orientation, leads to fork stalling, DNA damage, and cell death (Hamperl et al.,

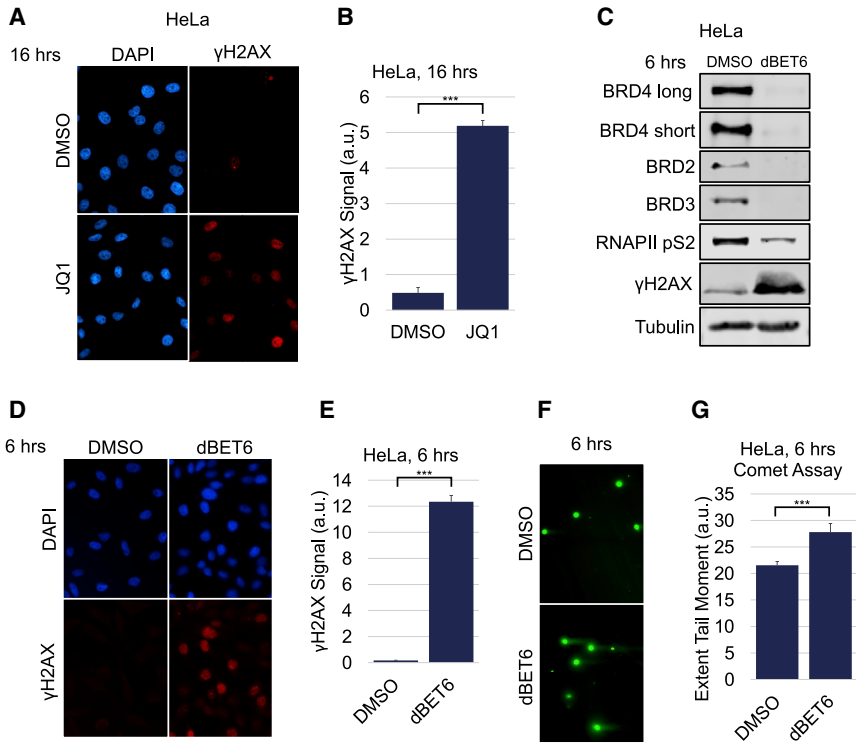

Figure 1. BET Protein LOF Leads to Spontaneous DNA Damage

(A and B) Representative images (A) and quantification (B) of γH2AX staining per nucleus in HeLa cells treated with DMSO or 500 nM JQ1 for 16 h (>100 cells).

(C) Representative western blots from HeLa cells treated with DMSO or 100 nM dBET6 for 6 h before harvest.

(D and E) Representative images (D) and quantification (E) of γH2AX staining per nucleus in HeLa cells treated with DMSO or 100 nM dBET6 for 6 h.

(F and G) Representative images (F) and quantification (G) of neutral single-cell electrophoresis assay of HeLa cells treated with DMSO or 100 nM dBET6 for 6 h.

(H) Representative western blots from HeLa cells treated with various BET inhibitors for 8 h before harvest.

For western blots, lysates are probed for the epitope indicated beside each panel. Student's t test (two-tailed, unpaired) was performed on (B), (E), and (G). Data represent the mean ± SEM. *$p < 0.05$; **$p < 0.01$; ***$p < 0.001$. Primary source data for this figure and for all subsequent figures and supplementary data can be found at https://data.mendeley.com/datasets/j4kdb59xyf/3.

2017). While probing for DNA damage following BET protein loss in immunofluorescence microscopy studies, we noticed heterogeneity in which cells would display γH2AX foci following dBET6 exposure. Prior work from other groups showed that BRD4 loss leads to a loss of S-phase cells (Maruyama et al., 2002). While this has been described as a G1/S phase arrest, we decided to test whether actively replicating S-phase cells could be prone to DNA damage after BRD4 loss.

To test whether BET protein loss leads to DNA damage preferentially in actively replicating cells, we labeled HeLa cells with EdU to monitor actively replicating cells while simultaneously treating with dBET6 for 2 hs. Accordingly, we observed that γH2AX foci formed only in the cells that were labeled with EdU by immunofluorescence (Figures 2A and 2B). We also labeled OCI-AML2 cells, another JQ1-sensitive cell line (Fiskus et al., 2014; Zhou et al., 2018), and saw that EdU-positive cells showed increased DNA damage following dBET6 treatment (Figures S2A and S2B). These data indicate that BET protein loss specifically leads to DNA damage in cells that are actively replicating in S-phase.

To determine whether the S-phase-specific DNA damage following BET loss of function (LOF) was associated with cell death, we performed cell-cycle analysis of HeLa cells treated with JQ1 or dBET6. Previous work has shown that apoptotic cells comprise a broad hypodiploid (sub-G_1) peak (Riccardi and Nicoletti, 2006) in flow cytometry experiments using propidium iodide to label nuclear DNA content. Interestingly, following BET LOF, we observed a decrease in the S-phase population of cells and a corresponding increase in the sub-G_1 population (Figures 2C–2E). These flow cytometry findings indicate that BET LOF leads to cell death of cells in S-phase.

These observations also correlated with replication stress and apoptotic signaling. RPA2, a downstream target of the replication stress master kinase ATR, is known to be phosphorylated on Serine 33 (RPA2-pS33) by ATR in response to replication stress (Olson et al., 2006). BET inhibition with dBET6 caused a robust increase in RPA2-pS33 (Figure 2F), indicating that BET inhibition causes replication stress and providing further evidence that BET protein loss leads to S-phase-dependent damage. Furthermore, in dBET6-treated cells, we saw increased levels of cleaved Poly(ADP-ribose) (cPARP), indicating that this S-phase damage was not effectively repaired and caused cell death (Figure 2F). Interestingly, we also saw elevated RPA-pS33 and apoptosis when murine KPR8 cells, which have a Kras G12D mutation and non-functional p53, were exposed to JQ1. In stark contrast, normal MEFs displayed no JQ1 response, demonstrating that BET-bromodomain inhibition elicits DNA damage, replication stress, and apoptosis in cells expressing oncogenic drivers (Figure S2C).

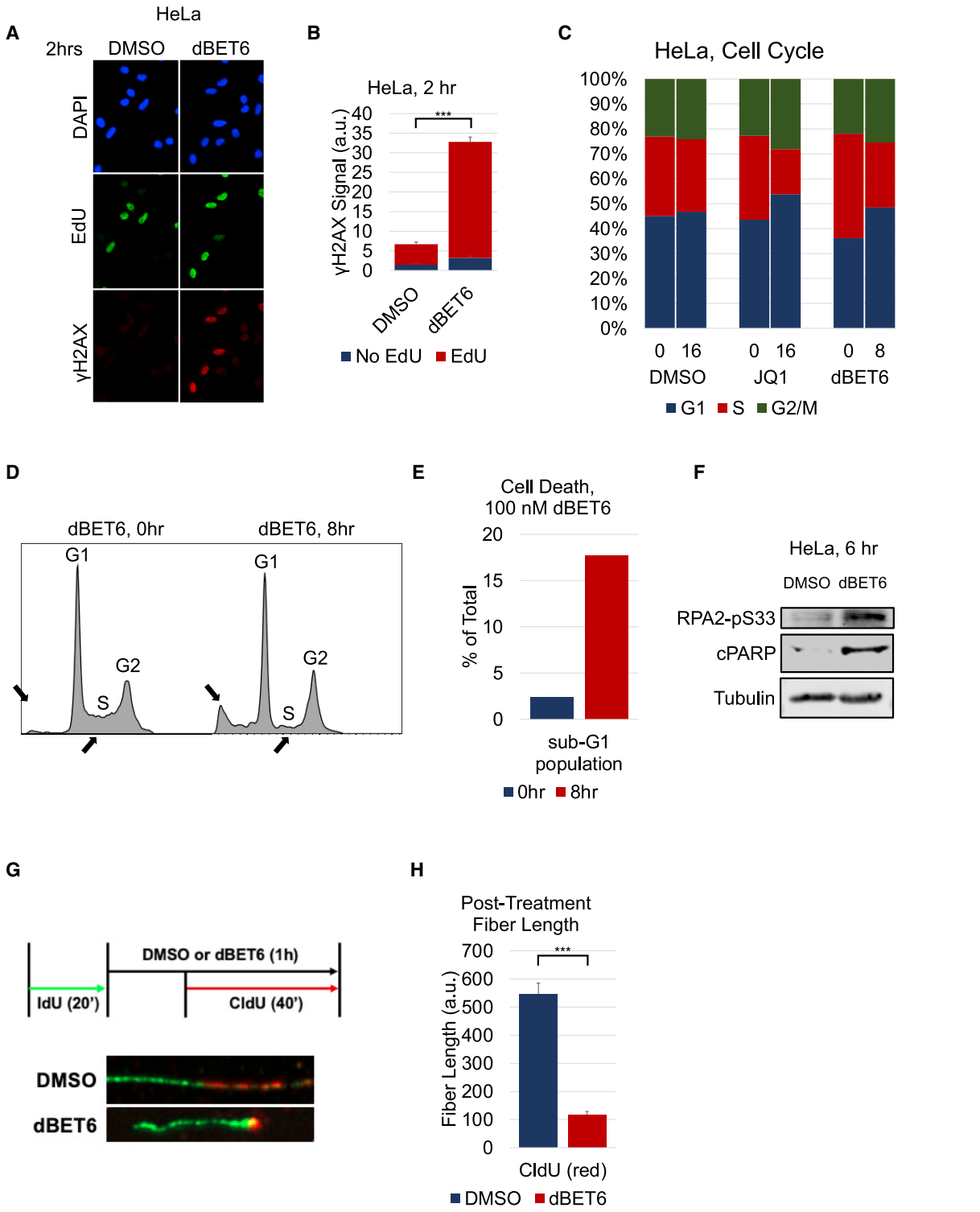

Figure 2. BET Protein Degradation Leads to Replication Stress and S-Phase-Dependent DNA Damage

(A and B) Representative images (A) and quantification (B) of γH2AX staining per nucleus in HeLa cells treated simultaneously with 100 nM dBET6 and 10 μM EdU for 2 h.

(C) Cell-cycle analysis of HeLa cells treated with DMSO, 500 nM JQ1, or 100 nM dBET6 for times as shown.

(D and E) Histogram (D) and quantification (E) of sub-G1 populations of HeLa cells before and after treatment with 100 nM dBET6.

(legend continued on next page)

Finally, to understand whether BET LOF led to dysregulation of replication, we used DNA fiber analysis to observe the progression of replication forks following treatment of dBET6. Interestingly, we found that treatment with dBET6 led to a significant decrease in CldU incorporation, indicating that BET LOF leads to a decrease in replication fork progression (Figures 2G and 2H). Taken together, these data demonstrate that BET LOF leads to an increase in replication stress and cell death in actively replicating cells.

The CTD of BRD4 Is Necessary to Prevent DNA Damage Caused by BET Protein Loss

The BET protein family consists of four members: BRD2, BRD3, BRD4, and BRDT (of note, BRDT is expressed mainly in the testes) (Pivot-Pajot et al., 2003). Inhibitors of this family of proteins—namely, JQ1 and the degrader dBET6—function by binding to the bromodomains that are shared by all members. Thus, it is important to elucidate how the various BET-bromodomain proteins contribute to the DNA damage seen by dBET6 treatment. To test this, we used small interfering RNA (siRNA) to specifically knock down BRD2, BRD3, or BRD4 and measured γH2AX signaling (Figures 3A and S3A). After 72 h of knockdown, we observed that both BRD2 and BRD4 loss led to increased γH2AX signaling, similar to recent reports (Kim et al., 2019). Owing to a wealth of studies that established mechanisms of BRD4 in transcription regulation and earlier work showing replication dysfunction caused by BRD4 loss (Bisgrove et al., 2007; Maruyama et al., 2002; Wessel et al., 2019; Winter et al., 2017), we focused on the role of BRD4 in the prevention of S-phase DNA damage.

The long isoform of BRD4 (BRD4L, Isoform A) contains several known domains, including two bromodomains, an extra-terminal domain, and a CTD (Figure 3B). The two bromodomains, which bind to acetylated lysine on histone tails, and the extra-terminal domain are shared among all BET protein members. The CTD, however, is unique to BRD4L and interacts with the P-TEFb complex that contains CDK9, leading to Serine 2 phosphorylation of RNAPII and transcription pause-release (Chen et al., 2014; Itzen et al., 2014; Jang et al., 2005; Kanno et al., 2014; Liu et al., 2013; Patel et al., 2013; Rahman et al., 2011; Winter et al., 2017; Zhang et al., 2012). As previous work showed that CDK9 inhibition leads to paused RNAPII and an increase in R-loops (Chen et al., 2019), we hypothesized that BRD4 loss could also lead to CDK9 dysfunction, resulting in DNA damage. Moreover, we reasoned that the P-TEFb-interacting CTD would be required to prevent TRCs and DNA damage.

To determine the mechanism behind damage caused by BET protein loss, we developed a panel of inducible BRD4-overexpression constructs and tested their ability to rescue the effects of dBET6 (Figure 3B). The panel included two naturally occurring isoforms that have previously been shown to carry out different functions: BRD4L, mentioned above, and BRD4 short isoform (BRD4S, Isoform C), which is truncated shortly after the extra-terminal domain. Added to this panel were two modified isoforms. The first was a modified short-isoform construct missing the extra-terminal domain (SΔET). The second was a truncated construct of the long isoform missing amino acids 1329–1362 of the CTD (LΔCTD). This deleted portion of the CTD was previously shown to interact with CDK9 (Bisgrove et al., 2007). These constructs were used to develop stable cell lines under doxycycline transcriptional control (Figure S3B).

In order to determine whether BRD4 was able to rescue the DNA damage effects caused by dBET6, we induced BRD4L expression with doxycycline for 24 h before treatment with dBET6. We found that BRD4L was indeed able to rescue the γH2AX signaling caused by dBET6 (Figures 3C, 3D, S3C, and S3D). We also observed that BRD4L was able to rescue the loss of RNAPIIpS2, indicating that overexpressing BRD4L was able to ensure efficient transcription elongation even in the presence of dBET6 (Figure 3C). These data suggest that BRD4L is sufficient in rescuing the effects of dBET6. Next, we applied the same conditions to the entire panel of BRD4-overexpression constructs by western blot (Figures 3C and 3D). Importantly, none of the other overexpression constructs were able to rescue either the γH2AX signaling or the loss of RNAPIIpS2. Furthermore, we saw that only BRD4L was able to rescue the S-phase-specific γH2AX foci caused by dBET6 treatment (Figures 3E and 3F). These observations indicate that the CTD is required to prevent BET-inhibitor-induced loss of RNAPIIpS2 and S-phase DNA damage.

To elucidate whether the CTD of BRD4 was necessary to rescue the DNA double-strand breaks caused by dBET6 treatment, we used a comet assay to quantify the breaks following dBET6 treatment following overexpression of BRD4L or LΔCTD. Again, we saw that BRD4L, but not LΔCTD, was able to rescue the dBET6-induced DNA double-strand breaks. This further indicates that the CTD of BRD4 is necessary to prevent DNA double-strand breaks in S-phase and points to a mechanism involving both transcription and replication.

BET Inhibition Leads to an Increase in R-Loop-Dependent DNA Damage

R-loops have been previously shown to cause TRCs and replication stress in cancer (Aguilera and Gómez-González, 2017; Costantino and Koshland, 2018; Crossley et al., 2019; García-Muse and Aguilera, 2019; Hamperl and Cimprich, 2016; Hamperl et al., 2017; Richard and Manley, 2017; Santos-Pereira and Aguilera, 2015; Sollier and Cimprich, 2015). Specifically, an R-loop is able to tether a persistently paused RNAPII to the chromatin, creating a roadblock for the replication machinery. RNAPII, after initiation of transcription of ~50 bp, becomes paused until a second phosphorylation event of the second serine on its tail. BRD4, through its CTD, activates CDK9 to cause this phosphorylation event and ensure efficient transcription elongation (Bisgrove

(F) Representative western blot images of lysates from HeLa cells treated with DMSO or 100 nM dBET6 for 6 h, probed for the epitope indicated beside each panel.

(G and H) Representative images (G) and quantification (H) of DNA fiber analysis of HeLa cells treated with DMSO or 100 nM dBET6.

Cells in (C)–(E) were fixed after treatment, stained with PI, and quantified for DNA content using flow cytometry. Student's t test (two-tailed, unpaired) was performed on (B) and (H). Data represent the mean ± SEM. *$p < 0.05$; **$p < 0.01$; ***$p < 0.001$.

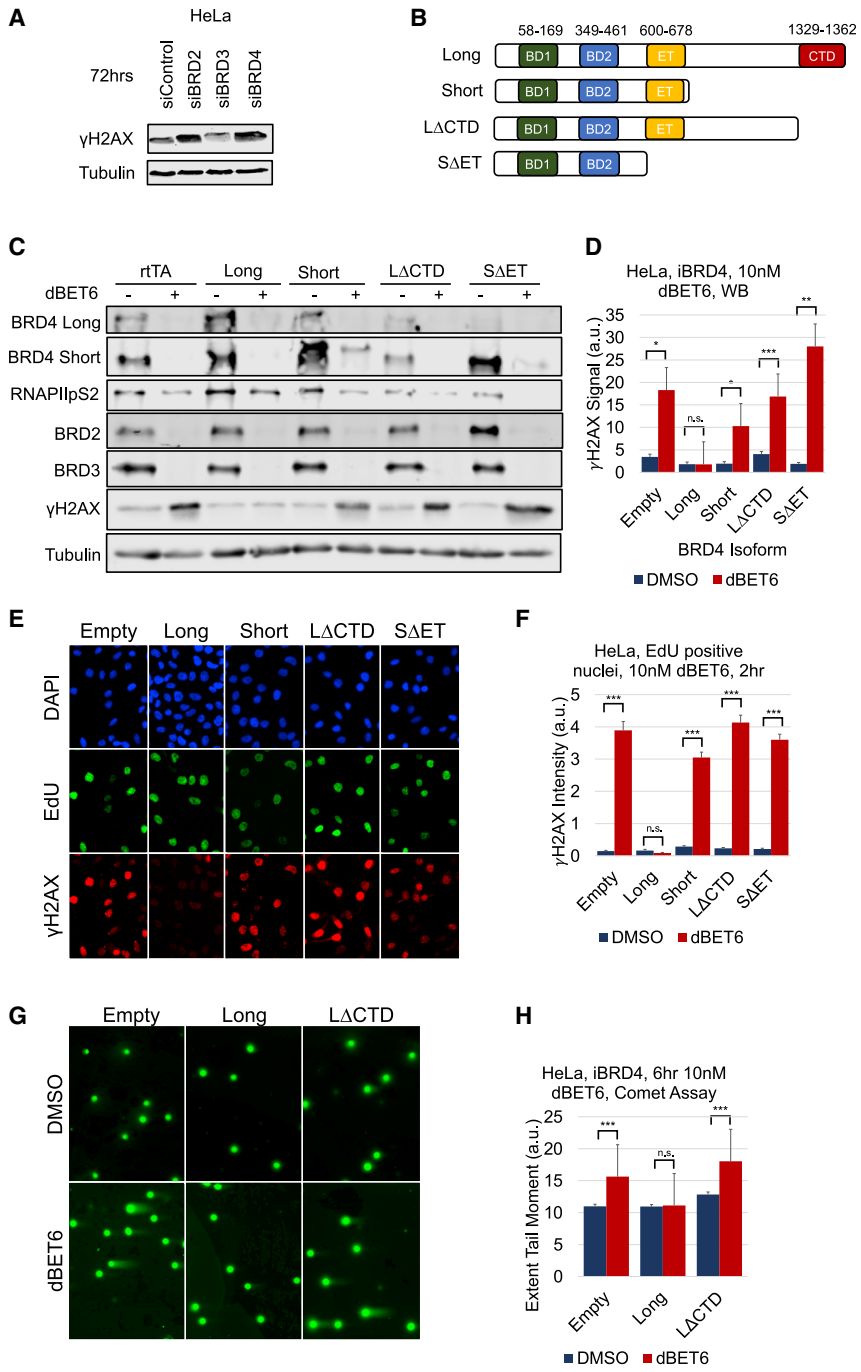

Figure 3. The CTD of BRD4 Is Required to Prevent TRCs

(A) Representative western blots of HeLa cells treated with siControl, siBRD2, siBRD3, or siBRD4 for 72 h and probed for the epitope indicated beside each panel.

(B) Domain structure of overexpression constructs depicting the location of the bromodomains, extra-terminal domain, and CTD of BRD4.

(C and D) Representative images (C) and quantification (D) of western blots from HeLa cells stably infected with each BRD4 construct and induced with doxycycline for 24 h before being treated with 10 nM dBET6 for 6 h and harvested. Lysates were probed for the epitope indicated beside each panel.

(E and F) Representative images (E) and quantification (F) of γH2AX staining per nucleus in EdU-positive HeLa cells induced as in (D) and then simultaneously treated with 10 nM dBET6 and 10 μM EdU for 2 h.

(G and H) Representative images (G) and quantification (H) of neutral single-cell electrophoresis assay of HeLa cells induced as in (D) followed by treatment with DMSO or 10 nM dBET6 for 6 h.

Student's t test (two-tailed, unpaired) was performed on (D), (F), and (H). Data represent the mean ± SEM. *p < 0.05; **p < 0.01; ***p < 0.001.

et al., 2007; Chen et al., 2014; Itzen et al., 2014; Jang et al., 2005; Krueger et al., 2010; Patel et al., 2013). Previous work has also shown that loss of BRD4 leads to decreased traveling ratios of RNAPII after dBET6 treatment, indicating that RNAPII is paused on the chromatin (Winter et al., 2017). Furthermore, previous studies have indicated that direct chemical inhibition of CDK9 leads to stalled RNAPII and an increase in R-loop formation (Chen et al., 2017; Shao and Zeitlinger, 2017). Therefore, we hypothesized that loss of BRD4 may also lead to an increase of R-loops, and those R-loops are responsible for the S-phase damage seen after BRD4 loss.

To determine whether BRD4 loss leads to an increase in R-loop formation, we employed the R-chromatin immunoprecipitation sequencing (ChIP-seq) technique, which has previously been described as a way to detect R-loop formation on the chromatin (Chen et al., 2019). R-ChIP employs the use of a catalytically inactive form of the R-loop-specific endonuclease, RNase H1. The mutation, D210N, allows RNase H1 to bind to, but not resolve, R-loops. The construct is tagged with a V5 peptide, which then allows it to be enriched from cross-linked cells, along with associated chromatin, for ChIP-seq (Figure S4A). We performed R-ChIP-seq in dBET6-exposed cells and found dramatic increases in global R-loop formation (Figure 4A). Similarly, we saw globally increased γH2AX ChIP signal in dBET6-treated cells. Furthermore, we validated three previously described (Liu et al., 2013) BRD4-occupying loci using R-ChIP-qPCR (Figures 4B and 4C). Surprisingly, while we saw most of the R-loop formation near the promoter regions, there was also increased R-loop formation throughout the length of the gene. In addition, we saw a decrease of RNAPIIpS2 along the length of these loci and an increase in RNAPII travel ratio, which has been reported previously (Winter et al., 2017) (Figures S4B and S4C). This indicates that BRD4

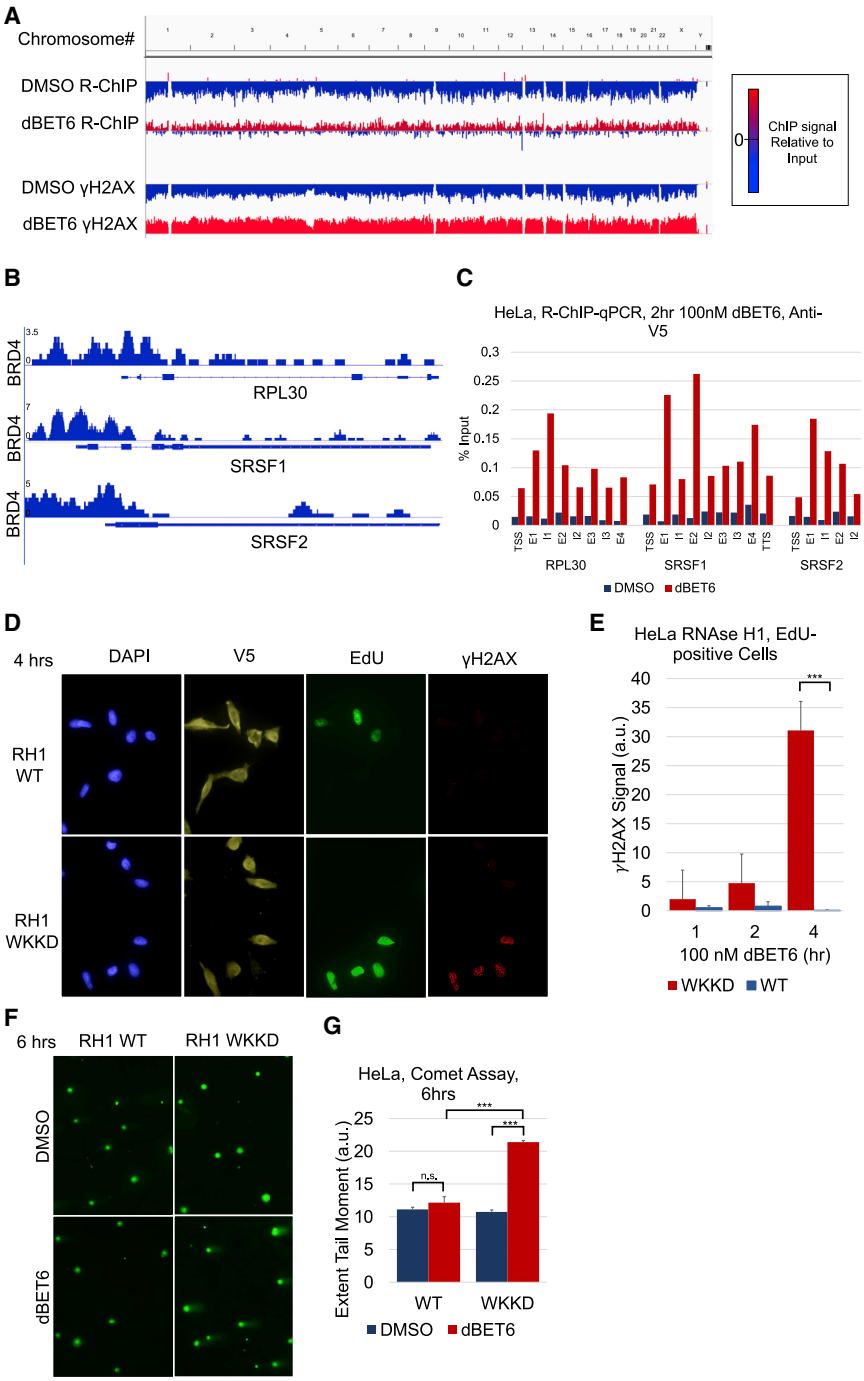

Figure 4. BET Inhibition Leads to an Increase in R-Loop-Dependent DNA Damage

(A) Global ChIP-seq and R-ChIP-seq signal relative to input for HeLa cells treated with DMSO or dBET6 as shown. The right panel depicts how different colors represent the ChIP-seq or R-ChIP-seq signal relative to input.

(B) BRD4 ChIP-seq signal of select loci from ChIP-seq data published in Liu et al. (2013).

(C) Quantification of R-ChIP-qPCR at loci shown in (B) after treatment with DMSO or 100 nM dBET6.

(D and E) Representative images (D) and quantification (E) of γH2AX staining per nucleus in HeLa cells transfected with WT or WKKD mutant RNase H1 before being treated with 100 nM dBET6 or 10 μM EdU for 4 h.

(F and G) Representative images (F) and quantification (G) of neutral single-cell electrophoresis assay of HeLa cells transfected as in (E) before treatment with DMSO or 100 nM dBET6 for 6 h. Student's t test (two-tailed, unpaired) was performed on (E). ANOVA was performed on (G). Data represent the mean ± SEM. *$p < 0.05$; **$p < 0.01$; ***$p < 0.001$.

prevents not only pause-release of RNAPII, but also the accumulation of R-loops and RNAPII stalling throughout the length of the gene.

We next postulated that the R-loops formed by BRD4 loss could be the root cause of the S-phase DNA damage we observed. To elucidate this, we employed the overexpression of V5-tagged wild-type (WT) RNase H1, which is known to be able to resolve R-loops and reverse DNA damage caused by their existence (Matos et al., 2019). As a negative control, we used a V5-tagged RNase H1 mutant, containing mutations at W43A, K59A, K60A, and D210N (WKKD), which has been previously described to lack both the catalytic activity and the DNA-binding activity of RNase H1 (Chen et al., 2017). To test whether RNase H1 was able to rescue the S-phase DNA damage caused by BRD4 loss, we overexpressed either the WT RNase H1 or the WKKD mutant construct, treated with dBET6, and stained for V5, EdU, and γH2AX (Figures 4D, 4E, and S4D). Consistent with our hypothesis that BET inhibition leads to DNA damage via increased formation of R-loops, overexpression of WT RNaseH1, but not the non-binding WKKD mutant, rescued the DNA damage induced by BRD4 loss in EdU-positive cells. We then sought to test whether RNase H1 was able to rescue the DNA double-strand breaks caused by dBET6 (Figures 4F and 4G). Similarly, we observed that RNase H1 was also able to rescue these DNA double-strand breaks. These data indicate that following BRD4 loss, R-loops form and lead to DNA damage in S-phase, likely from TRCs. We also note prior reports of Ras expression leading to R-loop induction and replication stress (Kotsantis et al., 2016). Accordingly, we observed elevated DNA damage and markers of replication stress in MEFs expressing mutant Kras (Figure S2C).

As BRD4 plays a regulatory role in the transcription of many genes, we sought to understand whether BRD4 was playing a

direct role in preventing R-loop formation or whether it was indirectly preventing R-loop formation through the transcriptional control of other proteins implicated in R-loop processing. SETX and SRSF1 have both been previously shown to be involved with R-loop processing (Li and Manley, 2005; Sollier et al., 2014). We saw that dBET6 treatment did not impact the level of SETX or SRSF1 in the time frame when the R-loop-dependent TRCs and DNA damage occurred (Figure S4E).

In order to dissect the mechanism of BET-LOF-induced TRCs and DNA damage, we explored whether knockdown of other proteins associated with transcription would have an effect on DNA damage caused by BET LOF. HEXIM normally holds CDK9 in an inhibitory complex until activated by BRD4 (Chen et al., 2014; Krueger et al., 2010). In addition, the nuclear excision factors XPG and XPF have been implicated in the resolution of R-loops in transcription termination (Sollier et al., 2014). Interestingly, knockdown of these proteins also did not have an effect on the DNA damage caused by dBET6 (Figures S4F and S4G).

Topoisomerases, which relieve torsional stress produced by the movement of both the replication fork and the transcription bubble, are important in preventing replication stress caused by TRCs (Bermejo et al., 2012; Tuduri et al., 2009). Specifically, the activity of Top1 has been implicated in relieving negative supercoiling behind a transcription bubble that can lead to R-loop formation (Drolet et al., 1995; El Hage et al., 2010; Kim et al., 2019; Massé et al., 1997). In addition, BET inhibition has been previously shown to kill cells synergistically with the topoisomerase 1 (Top1) inhibitor, camptothecin (Baranello et al., 2016; Wessel et al., 2019). We therefore measured DNA damage after Top1 inhibition alone or in combination with bromodomain degradation. As expected, exposing HeLa cells to either dBET6 or camptothecin alone results in DNA damage; however, the combination showed additive effects, indicating that BRD4 may be causing DNA damage through mechanisms in addition to Top1 inhibition (Figure S4H). Indeed, prior work indicates that BRD4-stimulated activation of Top1 proceeds through an N-terminal kinase activity (Baranello et al., 2016). Our data indicate that this N-terminal BRD4 activity is insufficient to rescue the TRC-driven DNA damage that we observe specifically in S-phase (Figure 3).

Interestingly, recent reports indicate that Top2 is required to produce DNA damage following BRD2 LOF (Kim et al., 2019). In contrast, we saw that Top2 inhibition with dexrazoxane combined with dBET6 in HeLa cells increased DNA damage signaling at proximal time points (Figure S4H). However, after siRNA knockdown of Top2α or Top2β for 48 h in HeLa cells, we observed an effect on the DNA damage caused by 6 h of dBET6 inhibition that did not reach statistical significance (Figures S4F and S4G). These findings point to a mechanism of S-phase-dependent DNA damage that is not as dependent on Top2 function and occurs rapidly following BET-bromodomain inhibition in cells with high replication and transcription activity.

Active Transcription and RNAPII Occupancy Are Required for BET-Protein-Loss-Induced Damage

There are five stages of transcription: RNAPII recruitment, initiation, pause/release, elongation, and termination (Haberle and Stark, 2018; Porrua and Libri, 2015). Transcription initiation is denoted by a phosphorylation event in which CDK7, a subunit of TFIIH, phosphorylates Serine 5 on the tail of RNAPII (Komarnitsky et al., 2000). After ~50 bp of nascent transcription, RNAPII undergoes a pausing event until CDK9, a subunit of P-TEFb, phosphorylates Serine 2 on the tail of RNAPII (Baumli et al., 2012). Inhibitors of these two kinases exist and have been shown to have different effects on RNAPII occupation of chromatin (Shao and Zeitlinger, 2017). Triptolide (TRP) inhibits TFIIH and results in the blocking of transcription initiation and the degradation of RNAPII (Figure S5A). DRB inhibits CDK9 and leads to loss of RNAPIIpS2 and stalling of RNAPII on the chromatin, resulting in R-loops and TRCs (Chen et al., 2017; Shao and Zeitlinger, 2017) (Figure S5B). With this understanding, we hypothesized that these two molecules would have differing effects on the DNA damage caused by BRD4 loss.

To test whether degradation of RNAPII with TRP would be able to rescue the DNA damage effects of dBET6 treatment, we designed an experiment to pre-treat and manipulate RNAPII prior to dBET6 exposure, as described in Figure 5A. After pre-treating with either TRP or DRB, we washed out the drugs and treated with dBET6 for 1 h. Following the dBET6 treatment, cells were fixed and stained for γH2AX (Figures 5B and 5C). Remarkably, we saw that TRP was able to rescue the DNA damage effects of dBET6, while DRB was not. We then co-treated HCT-116 cells with TRP and dBET6 and saw that TRP was also able to rescue the DNA damage effects caused by dBET6 in this cell line (Figures S5C and S5D). These data indicate that RNAPII occupation on the chromatin is necessary for DNA damage caused by BRD4 loss.

We also wanted to explore the relationship between RNAPIIpS2 and DNA damage caused by dBET6 treatment. We observed that when BRD4L is overexpressed, there is an increase in RNAPIIpS2 (Figure 5D). In addition, we see that RNAPIIpS2 negatively correlates with γH2AX following dBET6 treatment both in HeLa cells and HEK293T cells (Figures 5E, S5E, and S5F). These data again suggest that the loss of BRD4 leads to loss of transcription and pausing of RNAPII on the chromatin, causing TRCs and subsequent DNA damage.

DISCUSSION

Inhibitors of BRD4 have been shown to inhibit growth of several cancer cell types, yet the mechanism of action remains unclear (Asangani et al., 2014; Dawson et al., 2011; Rathert et al., 2015; Zuber et al., 2011). Specifically, questions remain as to the mechanism by which inhibition of BRD4, which controls global transcription (Winter et al., 2017), may preferentially impact cancer cells more than normal cells—a feature that is required of all effective chemotherapies. Here, we propose a novel role for BRD4 in the prevention of R-loops, TRCs, S-phase-dependent DNA damage, and cell death in highly transcription- and replication-driven cells.

Our data show that inhibition or degradation of BET proteins—with JQ1 or dBET6, respectively—leads to an accumulation of DNA damage signaling and DNA double-strand breaks. When we characterized the nature of the DNA damage, we found that in the several cell types we investigated, the cell-cycle state dictated whether a cell accumulated this damage. Specifically, we saw that cells actively undergoing replication in S-phase

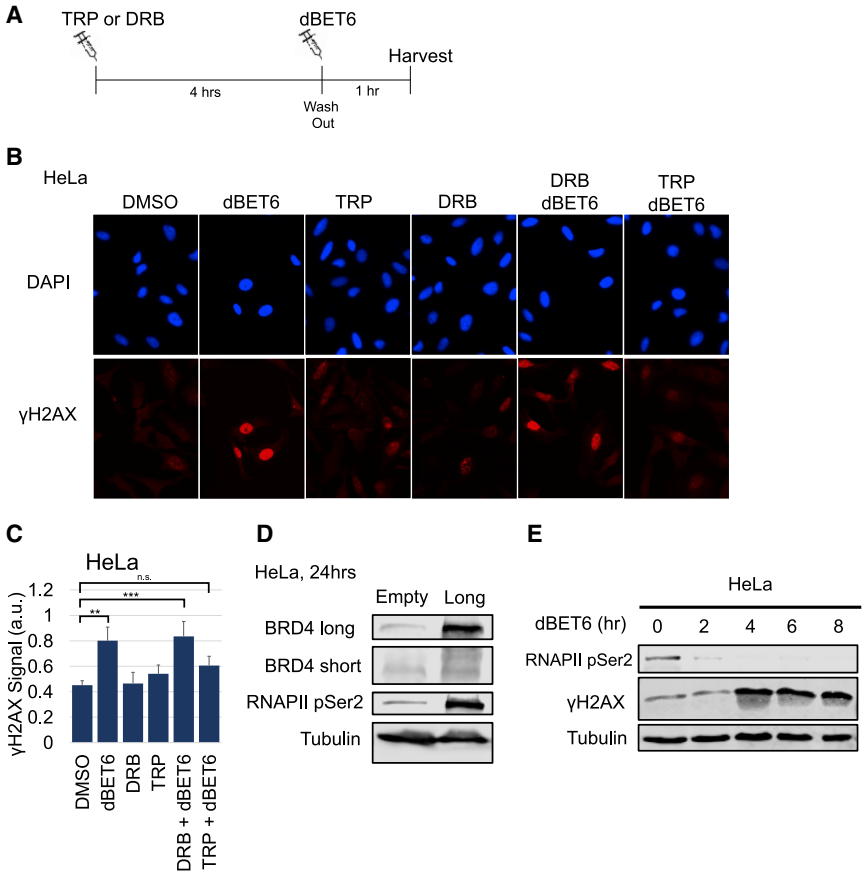

Figure 5. RNAPII Loss Rescues TRCs Caused by BET Inhibition

(A) Depiction of experimental design. HeLa cells were treated with 250 nM Triptolide or 100 μM DRB for 4 h before being washed out. Subsequently, cells were treated with 100 nM dBET6 for 1 h before fixation.

(B and C) Representative images (B) and quantification (C) of γH2AX staining per nucleus from HeLa cells treated as described in (A).

(D) Representative images of western blots from HeLa cells stably induced with the expression construct shown above each column for 24 h.

(E) Representative images of western blots from HeLa cells treated with 100 nM dBET6 for indicated times.

ANOVA was performed on (C). Data represent the mean ± SEM. *$p < 0.05$; **$p < 0.01$; ***$p < 0.001$.

preferentially exhibited DNA damage and cell death following BET protein LOF. Historically, BET proteins have been shown to play a major role in transcription regulation; thus, we postulated that the S-phase-dependent DNA damage caused by BET protein loss could be working through a mechanism of increased TRCs.

Because BET protein inhibitors such as JQ1 and degraders such as dBET6 target the bromodomains of BRD2, BRD3, and BRD4, it was previously unclear if one member of the family is responsible for the DNA damage caused by BET protein loss. Several works have shown that the different BET proteins have both unique and shared roles in the cell (Cheung et al., 2017; Hsu et al., 2017; LeRoy et al., 2008). Our data show that while siRNA-induced loss of either BRD2 or BRD4 caused increased γH2AX signaling after 72 h, overexpression of BRD4L was sufficient to effectively rescue the DNA damage effects of rapid BET protein degradation caused by dBET6. Specifically, we observed that the C-terminal P-TEFb-interacting domain of BRD4 was necessary to rescue this effect. Our data and the literature show that the CTD plays a critical role in the activation of RNAPII to ensure efficient elongation (Chen et al., 2014; Itzen et al., 2014; Jang et al., 2005; Kanno et al., 2014; Liu et al., 2013; Patel et al., 2013; Rahman et al., 2011; Winter et al., 2017; Zhang et al., 2012). BRD4, through its CTD, interacts with CDK9 to phosphorylate Serine 2 on the heptapeptide repeat on the tail of RNAPII. This phosphorylation event allows RNAPII to proceed with transcription elongation on schedule. Previous studies have identified DRB, a small-molecule inhibitor of CDK9, as a factor that increases R-loop formation (Chen et al., 2017). Our work adds to this finding by identifying BRD4, a physiological activator or CDK9, as an important R-loop regulator. Our findings show that BRD4 LOF causes S-phase-dependent DNA damage through a novel TRC mechanism, specifically in highly transcription-replication-driven cells. This novel mechanism is distinct from that proposed for BET-bromodomain proteins in other recent work (Bowry et al., 2018; Kim et al., 2019) and impacts the use of BET-bromodomain inhibitors, which are in clinical trials for a number of diseases.

In recent years, the importance of R-loops has become more apparent. While they play critical roles in normal physiological activity (Chaudhuri and Alt, 2004; García-Muse and Aguilera, 2019; Shao and Zeitlinger, 2017; Skourti-Stathaki and Proudfoot, 2014; Stuckey et al., 2015; Xiao et al., 2017), it has also come to light that aberrant R-loops can lead to TRCs, DNA damage, and cell death (Aguilera and Gómez-González, 2017; Costantino and Koshland, 2018; Crossley et al., 2019; García-Muse and Aguilera, 2019; Hamperl and Cimprich, 2016; Hamperl et al., 2017; Richard and Manley, 2017; Santos-Pereira and Aguilera, 2015; Sollier and Cimprich, 2015). Our data show that DNA damage caused by BRD4 loss is correlated with an increase in R-loop formation. Furthermore, this damage can be rescued by overexpressing RNase H1, an endonuclease that resolves R-loops. These observations indicate that some cells may depend on BRD4 to ensure that efficient transcription during S-phase prevents R-loop-dependent TRCs. We believe this is an important observation, especially as it pertains to cells with elevated replicative and transcriptional drive. Specifically, cancer cells and other highly driven cells may be more dependent on BRD4 to prevent the transcription and replication machinery from colliding. This finding may shed light on additional prior studies.

Early work on BRD4 knockout mice showed both embryonic lethality and replication deficits (Houzelstein et al., 2002; Maruyama et al., 2002). Additionally, studies of the normal tissue toxicities of whole-animal knockout of BRD4 could indicate vulnerability in rapidly replicating normal tissues (Bolden et al., 2014). Finally, it informs BET inhibition synergy with ATR inhibitors, resulting in increased γH2AX signaling and cell death (Pericole et al., 2019). Our proposed mechanism would predict that this synergy exists by increasing the number of TRCs while simultaneously inhibiting a cell's ability to handle replication stress.

One outstanding question that remains to be completely resolved is what makes a cell more or less sensitive to BRD4 loss. It has been shown that certain cancer cell lines are more sensitive to BET protein inhibition (Rathert et al., 2015), yet it is unclear as to why this is the case. For example, our group and others have shown that BRD4 loss in certain cell lines does not cause an increase in DNA damage signaling, while recent reports have identified cell lines that display DNA damage caused by BET-bromodomain protein inhibition (Bowry et al., 2018; Floyd et al., 2013; Kim et al., 2019). Notably, it is reported that that some cell lines do not exhibit a decrease in RNAPIIpS2 following BRD4 loss, and some R-loops formed by BET-bromodomain protein loss do not cause replication stress (Bowry et al., 2018; Kim et al., 2019). We hypothesize that some cancer cell lines may be more globally dependent on BRD4-mediated transcriptional activation. This can lead to R-loop formation, TRCs, DNA damage, and cell death upon BET inhibition. We believe that RNAPIIpS2 loss after BRD4 degradation could be predictive of whether a cancer cell line exhibits DNA damage following treatment. Through further study of both BRD4 and the role of R-loops in cancer, we hope that we can identify new therapeutic strategies and broaden the effectiveness of BET inhibitors against cancer.

Limitations

This manuscript was prepared, in part, during the COVID-19 pandemic that began in the spring of 2020. Therefore, we would like to address certain limitations to this work, as our ability to perform experiments was impacted during this time. Recent work has described the role of BRD2-mediated prevention of R-loop DNA damage through interactions with topoisomerases (Kim et al., 2019). It is likely that these findings co-exist with the findings described in this manuscript, but a cell's state (including replicative and transcriptional drive) plays a role in determining which mechanism predominates. While we were able to establish that such differences exist (Figures S4F–S4H), further experiments are needed to elucidate the differences observed and how cell state interacts with BET-bromodomain control of R-loop dynamics.

STAR★METHODS

Detailed methods are provided in the online version of this paper and include the following:

SUPPLEMENTAL INFORMATION

Supplemental Information can be found online at https://doi.org/10.1016/j.celrep.2020.108166.

ACKNOWLEDGMENTS

We thank Xiang-Dong Fu for providing the RNAse H1 constructs, Adam Karpf for providing the pCW57 construct, Nathanael Gray for providing dBET6, James Bradner for providing JQ1, Tyler Jacks for providing MEF and KPR8 cells, and Kris Wood for providing OCI-AML2 cells. We also thank Duke MSTP for providing funding for D.S.E. to conduct this work through the training grant T32GM007171. The work was also funded by Burroughs Wellcome Career Award for Medical Scientists and American Cancer Society Research Scholar Grant 133394-RSG-19-030-01-DMC to S.R.F.

AUTHOR CONTRIBUTIONS

D.S.E. and S.R.F. designed the project. D.E., R.M., J.P.T., J.J.H.P., E.B.-S., J.Luo, and J.Ling conducted the experiments. D.E., R.M., J.Luo, and S.R.F. analyzed the data. D.S.E. and S.R.F. wrote the manuscript.

DECLARATION OF INTERESTS

The authors declare no competing interests.

Received: November 27, 2019
Revised: April 13, 2020
Accepted: August 27, 2020
Published: September 22, 2020

REFERENCES

Aguilera, A., and Gómez-González, B. (2017). DNA-RNA hybrids: the risks of DNA breakage during transcription. Nat. Struct. Mol. Biol. *24*, 439–443.

Asangani, I.A., Dommeti, V.L., Wang, X., Malik, R., Cieslik, M., Yang, R., Escara-Wilke, J., Wilder-Romans, K., Dhanireddy, S., Engelke, C., et al. (2014). Therapeutic targeting of BET bromodomain proteins in castration-resistant prostate cancer. Nature *510*, 278–282.

Baranello, L., Wojtowicz, D., Cui, K., Devaiah, B.N., Chung, H.-J., Chan-Salis, K.Y., Guha, R., Wilson, K., Zhang, X., Zhang, H., et al. (2016). RNA Polymerase II Regulates Topoisomerase 1 Activity to Favor Efficient Transcription. Cell *165*, 357–371.

Barger, C.J., Branick, C., Chee, L., and Karpf, A.R. (2019). Pan-Cancer Analyses Reveal Genomic Features of FOXM1 Overexpression in Cancer. Cancers (Basel) *11*, 251.

Baumli, S., Hole, A.J., Wang, L.-Z., Noble, M.E.M., and Endicott, J.A. (2012). The CDK9 tail determines the reaction pathway of positive transcription elongation factor b. Structure *20*, 1788–1795.

Bermejo, R., Lai, M.S., and Foiani, M. (2012). Preventing replication stress to maintain genome stability: resolving conflicts between replication and transcription. Mol. Cell *45*, 710–718.

Bisgrove, D.A., Mahmoudi, T., Henklein, P., and Verdin, E. (2007). Conserved P-TEFb-interacting domain of BRD4 inhibits HIV transcription. Proc. Natl. Acad. Sci. USA *104*, 13690–13695.

Blackford, A.N., and Jackson, S.P. (2017). ATM, ATR, and DNA-PK: The Trinity at the Heart of the DNA Damage Response. Mol. Cell *66*, 801–817.

Bolden, J.E., Tasdemir, N., Dow, L.E., van Es, J.H., Wilkinson, J.E., Zhao, Z., Clevers, H., and Lowe, S.W. (2014). Inducible in vivo silencing of Brd4 identifies potential toxicities of sustained BET protein inhibition. Cell Rep. *8*, 1919–1929.

Bowry, A., Piberger, A.L., Rojas, P., Saponaro, M., and Petermann, E. (2018). BET Inhibition Induces HEXIM1- and RAD51-Dependent Conflicts between Transcription and Replication. Cell Rep. *25*, 2061–2069.e4.

Chaudhuri, J., and Alt, F.W. (2004). Class-switch recombination: interplay of transcription, DNA deamination and DNA repair. Nat. Rev. Immunol. *4*, 541–552.

Chen, R., Yik, J.H.N., Lew, Q.J., and Chao, S.-H. (2014). Brd4 and HEXIM1: multiple roles in P-TEFb regulation and cancer. BioMed Res. Int. *2014*, 232870.

Chen, L., Chen, J.-Y., Zhang, X., Gu, Y., Xiao, R., Shao, C., Tang, P., Qian, H., Luo, D., Li, H., et al. (2017). R-ChIP Using Inactive RNase H Reveals Dynamic Coupling of R-loops with Transcriptional Pausing at Gene Promoters. Mol. Cell *68*, 745–757.e5.

Chen, J.-Y., Zhang, X., Fu, X.-D., and Chen, L. (2019). R-ChIP for genome-wide mapping of R-loops by using catalytically inactive RNASEH1. Nat. Protoc. *14*, 1661–1685.

Cheung, K.L., Zhang, F., Jaganathan, A., Sharma, R., Zhang, Q., Konuma, T., Shen, T., Lee, J.-Y., Ren, C., Chen, C.-H., et al. (2017). Distinct Roles of Brd2 and Brd4 in Potentiating the Transcriptional Program for Th17 Cell Differentiation. Mol. Cell *65*, 1068–1080.e5.

Cimprich, K.A., and Cortez, D. (2008). ATR: an essential regulator of genome integrity. Nat. Rev. Mol. Cell Biol. *9*, 616–627.

Costantino, L., and Koshland, D. (2018). Genome-wide Map of R-Loop-Induced Damage Reveals How a Subset of R-Loops Contributes to Genomic Instability. Mol. Cell *71*, 487–497.e3.

Crossley, M.P., Bocek, M., and Cimprich, K.A. (2019). R-Loops as Cellular Regulators and Genomic Threats. Mol. Cell *73*, 398–411.

Dawson, M.A., Prinjha, R.K., Dittmann, A., Giotopoulos, G., Bantscheff, M., Chan, W.-I., Robson, S.C., Chung, C.-W., Hopf, C., Savitski, M.M., et al. (2011). Inhibition of BET recruitment to chromatin as an effective treatment for MLL-fusion leukaemia. Nature *478*, 529–533.

Delmore, J.E., Issa, G.C., Lemieux, M.E., Rahl, P.B., Shi, J., Jacobs, H.M., Kastritis, E., Gilpatrick, T., Paranal, R.M., Qi, J., et al. (2011). BET bromodomain inhibition as a therapeutic strategy to target c-Myc. Cell *146*, 904–917.

Drolet, M., Phoenix, P., Menzel, R., Massé, E., Liu, L.F., and Crouch, R.J. (1995). Overexpression of RNase H partially complements the growth defect of an Escherichia coli delta topA mutant: R-loop formation is a major problem in the absence of DNA topoisomerase I. Proc. Natl. Acad. Sci. USA *92*, 3526–3530.

El Hage, A., French, S.L., Beyer, A.L., and Tollervey, D. (2010). Loss of Topoisomerase I leads to R-loop-mediated transcriptional blocks during ribosomal RNA synthesis. Genes Dev. *24*, 1546–1558.

Faivre, E.J., McDaniel, K.F., Albert, D.H., Mantena, S.R., Plotnik, J.P., Wilcox, D., Zhang, L., Bui, M.H., Sheppard, G.S., Wang, L., et al. (2020). Selective inhibition of the BD2 bromodomain of BET proteins in prostate cancer. Nature *578*, 306–310.

Filippakopoulos, P., Qi, J., Picaud, S., Shen, Y., Smith, W.B., Fedorov, O., Morse, E.M., Keates, T., Hickman, T.T., Felletar, I., et al. (2010). Selective inhibition of BET bromodomains. Nature *468*, 1067–1073.

Filippakopoulos, P., Picaud, S., Mangos, M., Keates, T., Lambert, J.-P., Barsyte-Lovejoy, D., Felletar, I., Volkmer, R., Müller, S., Pawson, T., et al. (2012). Histone recognition and large-scale structural analysis of the human bromodomain family. Cell *149*, 214–231.

Fiskus, W., Sharma, S., Qi, J., Valenta, J.A., Schaub, L.J., Shah, B., Peth, K., Portier, B.P., Rodriguez, M., Devaraj, S.G.T., et al. (2014). Highly active combination of BRD4 antagonist and histone deacetylase inhibitor against human acute myelogenous leukemia cells. Mol. Cancer Ther. *13*, 1142–1154.

Floyd, S.R., Pacold, M.E., Huang, Q., Clarke, S.M., Lam, F.C., Cannell, I.G., Bryson, B.D., Rameseder, J., Lee, M.J., Blake, E.J., et al. (2013). The bromodomain protein Brd4 insulates chromatin from DNA damage signalling. Nature *498*, 246–250.

Gaillard, H., and Aguilera, A. (2016). Transcription as a Threat to Genome Integrity. Annu. Rev. Biochem. *85*, 291–317.

Gan, W., Guan, Z., Liu, J., Gui, T., Shen, K., Manley, J.L., and Li, X. (2011). R-loop-mediated genomic instability is caused by impairment of replication fork progression. Genes Dev. *25*, 2041–2056.

García-Muse, T., and Aguilera, A. (2016). Transcription-replication conflicts: how they occur and how they are resolved. Nat. Rev. Mol. Cell Biol. *17*, 553–563.

García-Muse, T., and Aguilera, A. (2019). R Loops: From Physiological to Pathological Roles. Cell *179*, 604–618.

Grunseich, C., Wang, I.X., Watts, J.A., Burdick, J.T., Guber, R.D., Zhu, Z., Bruzel, A., Lanman, T., Chen, K., Schindler, A.B., et al. (2018). Senataxin Mutation Reveals How R-Loops Promote Transcription by Blocking DNA Methylation at Gene Promoters. Mol. Cell *69*, 426–437.e7.

Haberle, V., and Stark, A. (2018). Eukaryotic core promoters and the functional basis of transcription initiation. Nat. Rev. Mol. Cell Biol. *19*, 621–637.

Hamperl, S., and Cimprich, K.A. (2016). Conflict Resolution in the Genome: How Transcription and Replication Make It Work. Cell *167*, 1455–1467.

Hamperl, S., Bocek, M.J., Saldivar, J.C., Swigut, T., and Cimprich, K.A. (2017). Transcription-Replication Conflict Orientation Modulates R-Loop Levels and Activates Distinct DNA Damage Responses. Cell *170*, 774–786.e19.

Hanahan, D., and Weinberg, R.A. (2011). Hallmarks of cancer: the next generation. Cell *144*, 646–674.

Houzelstein, D., Bullock, S.L., Lynch, D.E., Grigorieva, E.F., Wilson, V.A., and Beddington, R.S.P. (2002). Growth and early postimplantation defects in mice deficient for the bromodomain-containing protein Brd4. Mol. Cell. Biol. *22*, 3794–3802.

Hsu, S.C., Gilgenast, T.G., Bartman, C.R., Edwards, C.R., Stonestrom, A.J., Huang, P., Emerson, D.J., Evans, P., Werner, M.T., Keller, C.A., et al. (2017). The BET Protein BRD2 Cooperates with CTCF to Enforce Transcriptional and Architectural Boundaries. Mol. Cell *66*, 102–116.e7.

Itzen, F., Greifenberg, A.K., Bösken, C.A., and Geyer, M. (2014). Brd4 activates P-TEFb for RNA polymerase II CTD phosphorylation. Nucleic Acids Res. *42*, 7577–7590.

Jang, M.K., Mochizuki, K., Zhou, M., Jeong, H.-S., Brady, J.N., and Ozato, K. (2005). The bromodomain protein Brd4 is a positive regulatory component of P-TEFb and stimulates RNA polymerase II-dependent transcription. Mol. Cell *19*, 523–534.

Kanno, T., Kanno, Y., LeRoy, G., Campos, E., Sun, H.-W., Brooks, S.R., Vahedi, G., Heightman, T.D., Garcia, B.A., Reinberg, D., et al. (2014). BRD4 assists elongation of both coding and enhancer RNAs by interacting with acetylated histones. Nat. Struct. Mol. Biol. *21*, 1047–1057.

Kim, J.J., Lee, S.Y., Gong, F., Battenhouse, A.M., Boutz, D.R., Bashyal, A., Refvik, S.T., Chiang, C.-M., Xhemalce, B., Paull, T.T., et al. (2019). Systematic bromodomain protein screens identify homologous recombination and R-loop suppression pathways involved in genome integrity. Genes Dev. *33*, 1751–1774.

Komarnitsky, P., Cho, E.J., and Buratowski, S. (2000). Different phosphorylated forms of RNA polymerase II and associated mRNA processing factors during transcription. Genes Dev. *14*, 2452–2460.

Kotsantis, P., Silva, L.M., Irmscher, S., Jones, R.M., Folkes, L., Gromak, N., and Petermann, E. (2016). Increased global transcription activity as a mechanism of replication stress in cancer. Nat. Commun. *7*, 13087.

Krueger, B.J., Varzavand, K., Cooper, J.J., and Price, D.H. (2010). The mechanism of release of P-TEFb and HEXIM1 from the 7SK snRNP by viral and cellular activators includes a conformational change in 7SK. PLoS ONE *5*, e12335.

LeRoy, G., Rickards, B., and Flint, S.J. (2008). The double bromodomain proteins Brd2 and Brd3 couple histone acetylation to transcription. Mol. Cell *30*, 51–60.

Li, X., and Manley, J.L. (2005). Inactivation of the SR protein splicing factor ASF/SF2 results in genomic instability. Cell *122*, 365–378.

Liu, W., Ma, Q., Wong, K., Li, W., Ohgi, K., Zhang, J., Aggarwal, A., and Rosenfeld, M.G. (2013). Brd4 and JMJD6-associated anti-pause enhancers in regulation of transcriptional pause release. Cell *155*, 1581–1595.

Lu, J., Qian, Y., Altieri, M., Dong, H., Wang, J., Raina, K., Hines, J., Winkler, J.D., Crew, A.P., Coleman, K., and Crews, C.M. (2015). Hijacking the E3 Ubiquitin Ligase Cereblon to Efficiently Target BRD4. Chem. Biol. *22*, 755–763.

Maruyama, T., Farina, A., Dey, A., Cheong, J., Bermudez, V.P., Tamura, T., Sciortino, S., Shuman, J., Hurwitz, J., and Ozato, K. (2002). A Mammalian bromodomain protein, brd4, interacts with replication factor C and inhibits progression to S phase. Mol. Cell. Biol. *22*, 6509–6520.

Massé, E., Phoenix, P., and Drolet, M. (1997). DNA topoisomerases regulate R-loop formation during transcription of the rrnB operon in Escherichia coli. J. Biol. Chem. *272*, 12816–12823.

Matos, D.A., Zhang, J.-M., Ouyang, J., Nguyen, H.D., Genois, M.-M., and Zou, L. (2019). ATR Protects the Genome against R Loops through a MUS81-Triggered Feedback Loop. Mol. Cell *77*, 514–527.e4.

McQuin, C., Goodman, A., Chernyshev, V., Kamentsky, L., Cimini, B.A., Karhohs, K.W., Doan, M., Ding, L., Rafelski, S.M., Thirstrup, D., et al. (2018). CellProfiler 3.0: Next-generation image processing for biology. PLoS Biol. *16*, e2005970.

Morales, J.C., Richard, P., Patidar, P.L., Motea, E.A., Dang, T.T., Manley, J.L., and Boothman, D.A. (2016). XRN2 Links Transcription Termination to DNA Damage and Replication Stress. PLoS Genet. *12*, e1006107.

Muhar, M., Ebert, A., Neumann, T., Umkehrer, C., Jude, J., Wieshofer, C., Rescheneder, P., Lipp, J.J., Herzog, V.A., Reichholf, B., et al. (2018). SLAM-seq defines direct gene-regulatory functions of the BRD4-MYC axis. Science *360*, 800–805.

Nguyen, H.D., Yadav, T., Giri, S., Saez, B., Graubert, T.A., and Zou, L. (2017). Functions of Replication Protein A as a Sensor of R Loops and a Regulator of RNaseH1. Mol. Cell *65*, 832–847.e4.

Odore, E., Lokiec, F., Cvitkovic, E., Bekradda, M., Herait, P., Bourdel, F., Kahatt, C., Raffoux, E., Stathis, A., Thieblemont, C., et al. (2016). Phase I Population Pharmacokinetic Assessment of the Oral Bromodomain Inhibitor OTX015 in Patients with Haematologic Malignancies. Clin. Pharmacokinet. *55*, 397–405.

Olson, E., Nievera, C.J., Klimovich, V., Fanning, E., and Wu, X. (2006). RPA2 is a direct downstream target for ATR to regulate the S-phase checkpoint. J. Biol. Chem. *281*, 39517–39533.

Ozer, H.G., El-Gamal, D., Powell, B., Hing, Z.A., Blachly, J.S., Harrington, B., Mitchell, S., Grieselhuber, N.R., Williams, K., Lai, T.-H., et al. (2018). BRD4 Profiling Identifies Critical Chronic Lymphocytic Leukemia Oncogenic Circuits and Reveals Sensitivity to PLX51107, a Novel Structurally Distinct BET Inhibitor. Cancer Discov. *8*, 458–477.

Parajuli, S., Tealsey, D.C., Murali, B., Jackson, J., Vindigni, A., and Stewart, S.A. (2017). Human Ribonuclease H1 resolves R loops and thereby enables progression of the DNA replication fork. J. Biol. Chem. *292*, 15216–15224.

Patel, M.C., Debrosse, M., Smith, M., Dey, A., Huynh, W., Sarai, N., Heightman, T.D., Tamura, T., and Ozato, K. (2013). BRD4 coordinates recruitment of pause release factor P-TEFb and the pausing complex NELF/DSIF to regulate transcription elongation of interferon-stimulated genes. Mol. Cell. Biol. *33*, 2497–2507.

Pericole, F.V., Lazarini, M., de Paiva, L.B., Duarte, A.D.S.S., Vieira Ferro, K.P., Niemann, F.S., Roversi, F.M., and Olalla Saad, S.T. (2019). BRD4 Inhibition Enhances Azacitidine Efficacy in Acute Myeloid Leukemia and Myelodysplastic Syndromes. Front. Oncol. *9*, 16.

Pivot-Pajot, C., Caron, C., Govin, J., Vion, A., Rousseaux, S., and Khochbin, S. (2003). Acetylation-dependent chromatin reorganization by BRDT, a testis-specific bromodomain-containing protein. Mol. Cell. Biol. *23*, 5354–5365.

Porrua, O., and Libri, D. (2015). Transcription termination and the control of the transcriptome: why, where and how to stop. Nat. Rev. Mol. Cell Biol. *16*, 190–202.

Quinet, A., Carvajal-Maldonado, D., Lemacon, D., and Vindigni, A. (2017). DNA Fiber Analysis: Mind the Gap!. Methods Enzymol. *591*, 55–82.

Rahman, S., Sowa, M.E., Ottinger, M., Smith, J.A., Shi, Y., Harper, J.W., and Howley, P.M. (2011). The Brd4 extraterminal domain confers transcription activation independent of pTEFb by recruiting multiple proteins, including NSD3. Mol. Cell. Biol. *31*, 2641–2652.

Ramírez, F., Ryan, D.P., Grüning, B., Bhardwaj, V., Kilpert, F., Richter, A.S., Heyne, S., Dündar, F., and Manke, T. (2016). deepTools2: a next generation web server for deep-sequencing data analysis. Nucleic Acids Res. *44*, W160-5.

Rathert, P., Roth, M., Neumann, T., Muerdter, F., Roe, J.-S., Muhar, M., Deswal, S., Cerny-Reiterer, S., Peter, B., Jude, J., et al. (2015). Transcriptional plasticity promotes primary and acquired resistance to BET inhibition. Nature *525*, 543–547.

Riccardi, C., and Nicoletti, I. (2006). Analysis of apoptosis by propidium iodide staining and flow cytometry. Nat. Protoc. *1*, 1458–1461.

Richard, P., and Manley, J.L. (2017). R Loops and Links to Human Disease. J. Mol. Biol. *429*, 3168–3180.

Robinson, J.T., Thorvaldsdóttir, H., Winckler, W., Guttman, M., Lander, E.S., Getz, G., and Mesirov, J.P. (2011). Integrative genomics viewer. Nat. Biotechnol. *29*, 24–26.

Rogakou, E.P., Pilch, D.R., Orr, A.H., Ivanova, V.S., and Bonner, W.M. (1998). DNA double-stranded breaks induce histone H2AX phosphorylation on serine 139. J. Biol. Chem. *273*, 5858–5868.

Santos-Pereira, J.M., and Aguilera, A. (2015). R loops: new modulators of genome dynamics and function. Nat. Rev. Genet. *16*, 583–597.

Schröder, S., Cho, S., Zeng, L., Zhang, Q., Kaehlcke, K., Mak, L., Lau, J., Bisgrove, D., Schnölzer, M., Verdin, E., et al. (2012). Two-pronged binding with bromodomain-containing protein 4 liberates positive transcription elongation factor b from inactive ribonucleoprotein complexes. J. Biol. Chem. *287*, 1090–1099.

Schwab, R.A., Nieminuszczy, J., Shah, F., Langton, J., Lopez Martinez, D., Liang, C.-C., Cohn, M.A., Gibbons, R.J., Deans, A.J., and Niedzwiedz, W. (2015). The Fanconi Anemia Pathway Maintains Genome Stability by Coordinating Replication and Transcription. Mol. Cell *60*, 351–361.

Shao, W., and Zeitlinger, J. (2017). Paused RNA polymerase II inhibits new transcriptional initiation. Nat. Genet. *49*, 1045–1051.

Shivji, M.K.K., Renaudin, X., Williams, Ç.H., and Venkitaraman, A.R. (2018). BRCA2 Regulates Transcription Elongation by RNA Polymerase II to Prevent R-Loop Accumulation. Cell Rep. *22*, 1031–1039.

Skourti-Stathaki, K., and Proudfoot, N.J. (2014). A double-edged sword: R loops as threats to genome integrity and powerful regulators of gene expression. Genes Dev. *28*, 1384–1396.

Skourti-Stathaki, K., Proudfoot, N.J., and Gromak, N. (2011). Human senataxin resolves RNA/DNA hybrids formed at transcriptional pause sites to promote Xrn2-dependent termination. Mol. Cell *42*, 794–805.

Sollier, J., and Cimprich, K.A. (2015). Breaking bad: R-loops and genome integrity. Trends Cell Biol. *25*, 514–522.

Sollier, J., Stork, C.T., García-Rubio, M.L., Paulsen, R.D., Aguilera, A., and Cimprich, K.A. (2014). Transcription-coupled nucleotide excision repair factors promote R-loop-induced genome instability. Mol. Cell *56*, 777–785.

Stork, C.T., Bocek, M., Crossley, M.P., Sollier, J., Sanz, L.A., Chédin, F., Swigut, T., and Cimprich, K.A. (2016). Co-transcriptional R-loops are the main cause of estrogen-induced DNA damage. eLife *5*, e17548.

Stuckey, R., García-Rodríguez, N., Aguilera, A., and Wellinger, R.E. (2015). Role for RNA:DNA hybrids in origin-independent replication priming in a eukaryotic system. Proc. Natl. Acad. Sci. USA *112*, 5779–5784.

Sun, C., Yin, J., Fang, Y., Chen, J., Jeong, K.J., Chen, X., Vellano, C.P., Ju, Z., Zhao, W., Zhang, D., et al. (2018). BRD4 Inhibition Is Synthetic Lethal with PARP Inhibitors through the Induction of Homologous Recombination Deficiency. Cancer Cell *33*, 401–416.e8.

Tuduri, S., Crabbé, L., Conti, C., Tourrière, H., Holtgreve-Grez, H., Jauch, A., Pantesco, V., De Vos, J., Thomas, A., Theillet, C., et al. (2009). Topoisomerase I suppresses genomic instability by preventing interference between replication and transcription. Nat. Cell Biol. *11*, 1315–1324.

Wahba, L., Amon, J.D., Koshland, D., and Vuica-Ross, M. (2011). RNase H and multiple RNA biogenesis factors cooperate to prevent RNA:DNA hybrids from generating genome instability. Mol. Cell *44*, 978–988.

Wessel, S.R., Mohni, K.N., Luzwick, J.W., Dungrawala, H., and Cortez, D. (2019). Functional Analysis of the Replication Fork Proteome Identifies BET Proteins as PCNA Regulators. Cell Rep. *28*, 3497–3509.e4.

Winter, G.E., Mayer, A., Buckley, D.L., Erb, M.A., Roderick, J.E., Vittori, S., Reyes, J.M., di Iulio, J., Souza, A., Ott, C.J., et al. (2017). BET Bromodomain Proteins Function as Master Transcription Elongation Factors Independent of CDK9 Recruitment. Mol. Cell *67*, 5–18.e19.

Xiao, Y., Luo, M., Hayes, R.P., Kim, J., Ng, S., Ding, F., Liao, M., and Ke, A. (2017). Structure Basis for Directional R-loop Formation and Substrate Handover Mechanisms in Type I CRISPR-Cas System. Cell *170*, 48–60.e11.

Zatreanu, D., Han, Z., Mitter, R., Tumini, E., Williams, H., Gregersen, L., Dirac-Svejstrup, A.B., Roma, S., Stewart, A., Aguilera, A., and Svejstrup, J.Q. (2019). Elongation Factor TFIIS Prevents Transcription Stress and R-Loop Accumulation to Maintain Genome Stability. Mol. Cell *76*, 57–69.e9.

Zeman, M.K., and Cimprich, K.A. (2014). Causes and consequences of replication stress. Nat. Cell Biol. *16*, 2–9.

Zhang, W., Prakash, C., Sum, C., Gong, Y., Li, Y., Kwok, J.J.T., Thiessen, N., Pettersson, S., Jones, S.J.M., Knapp, S., et al. (2012). Bromodomain-containing protein 4 (BRD4) regulates RNA polymerase II serine 2 phosphorylation in human CD4+ T cells. J. Biol. Chem. *287*, 43137–43155.

Zhang, J., Dulak, A.M., Hattersley, M.M., Willis, B.S., Nikkilä, J., Wang, A., Lau, A., Reimer, C., Zinda, M., Fawell, S.E., et al. (2018). BRD4 facilitates replication stress-induced DNA damage response. Oncogene *37*, 3763–3777.

Zhou, Y., Zhou, J., Lu, X., Tan, T.-Z., and Chng, W.-J. (2018). BET Bromodomain inhibition promotes De-repression of TXNIP and activation of ASK1-MAPK pathway in acute myeloid leukemia. BMC Cancer *18*, 731.

Zuber, J., Shi, J., Wang, E., Rappaport, A.R., Herrmann, H., Sison, E.A., Magoon, D., Qi, J., Blatt, K., Wunderlich, M., et al. (2011). RNAi screen identifies Brd4 as a therapeutic target in acute myeloid leukaemia. Nature *478*, 524–528.

STAR★METHODS

KEY RESOURCES TABLE

REAGENT or RESOURCE	SOURCE	IDENTIFIER
Antibodies		
Rabbit monoclonal anti-BRD4 N terminus	Abcam	Cat# ab128874, RRID:AB_11145462
Rabbit monoclonal anti-BRD2	Cell Signaling Technology	Cat# 5848, RRID:AB_10835146
Mouse monoclonal anti-BRD3	Abcam	Cat# ab50818, RRID:AB_868478
Rat monoclonal anti-RNA polymerase II phospho CTD Ser-2 (RNAPIIpS2)	Millipore	Cat# 04-1571, RRID:AB_10627998
Rabbit monoclonal anti-Histone H2A.X phospho Ser-139 (γH2AX)	Cell Signaling Technology	Cat# 9718, RRID:AB_2118009
Rabbit polyclonal anti-Histone H2A.X phospho Ser-139 (γH2AX)	Abcam	Cat# ab2893, RRID:AB_303388
Rabbit polyclonal anti-alpha Tubulin	Cell Signaling Technology	Cat# 2144, RRID:AB_2210548
Rabbit polyclonal anti-RPA32 phospho Ser-33 (RPApS33)	Abcam	Cat# ab211877, RRID:AB_2818947
Rabbit monoclonal anti-cleaved PARP (Asp214)	Cell Signaling Technology	Cat# 5625, RRID:AB_10699459
Rabbit monoclonal anti-CC3	Cell Signaling Technology	Cat# 9664, RRID:AB_2070042
Mouse monoclonal anti-BrdU	BD Biosciences	Cat# 347580, RRID:AB_10015219
Rat monoclonal anti-BrdU	Abcam	Cat# ab6326, RRID:AB_305426
Rabbit monoclonal anti-V5	Abcam	Cat# ab9116, RRID:AB_307024
Rabbit polyclonal anti-Senataxin (SETX)	Abcam	Cat# ab220827, RRID:AB_2818949
Mouse monoclonal anti-SRSF1	Thermo Fisher Scientific	Cat# 32-4600, RRID:AB_2533080
Mouse monoclonal anti-RNA polymerase II CTD (Total RNAPII)	Abcam	Cat# ab817, RRID:AB_306327
Rabbit polyclonal anti-DHX9	Thermo Fisher Scientific	Cat# PA519542, RRID:AB_10987556
Rabbit polyclonal anti-HEXIM1	Abcam	Cat# ab25388, RRID:AB_2233058
Rabbit monoclonal anti-topoisomerase II alpha	Abcam	Cat# ab52934, RRID:AB_883143
Rabbit polyclonal anti-topoisomerase II beta	Abcam	Cat# ab72334, RRID:AB_1271267
Rabbit polyclonal anti-XPF	Abcam	Cat# ab76948, RRID:AB_1524575
Rabbit polyclonal anti-XPG	Abcam	Cat# ab224815, RRID:AB_2861354
Goat Anti-Rabbit IgG 800CW	LI-COR Biosciences	Cat# 926-32211, RRID:AB_621843
Goat Anti-Mouse IgG 680RD	LI-COR Biosciences	Cat# 926-68070, RRID:AB_10956588
Goat Anti-Rat IgG 680LT	LI-COR Biosciences	Cat# 926-68029, RRID:AB_10715073
Goat Anti-Rabbit IgG Alexa Fluor 647	Life Technologies	Cat# A211245, RRID:AB_2535813
Goat Anti-Rabbit IgG Alexa Fluor 555	Invitrogen	Cat# A-21428, RRID:AB_2535849
Goat Anti-Rabbit IgG Alexa Fluor 488	Life Technologies	Cat# A-11008, RRID:AB_143165
Goat Anti-Mouse IgG Alexa Fluor 488	Invitrogen	Cat# A-11001, RRID:AB_2534069
Goat Anti-Rat IgG Alexa Fluor 647	Invitrogen	Cat# A-21247, RRID:AB_141778
Chemicals, Peptides, and Recombinant Proteins		
JQ1	Laboratory of James Bradner	Filippakopoulos et al., 2010
dBET6	Laboratory of Nathaneal Gray	Winter et al., 2017
Doxycycline	Sigma-Aldrich	Cat# D3447
Triptolide	Millipore	Cat# 645900
DRB	Cayman Chemical Company	Cat# 10010302

(*Continued on next page*)

Continued

REAGENT or RESOURCE	SOURCE	IDENTIFIER
Camptothecin	Selleck Chemicals	Cat# S1288
Dexrazoxane	Selleck Chemicals	Cat# S5651
OTX015	Selleck Chemicals	Cat# S7360
ABBV-075	Selleck Chemicals	Cat# S8400
ABBV-744	Selleck Chemicals	Cat# S8723
PLX51107	Selleck Chemicals	Cat# S8739
Critical Commercial Assays		
EdU-Click 488 kit	Sigma-Aldrich	Cat# BCK-EDU488
CometAssay Single Cell Electrophoresis kit	Trevigen	Cat# 4250-050-K
SimpleChIP Plus Sonication kit	Cell Signaling Technology	Cat# 56383S
LI-COR Revert 700 Total Protein	LI-COR Biosciences	Cat# 926-11016
Deposited Data		
Sequencing Data	This paper	GEO accession: GSE141763
Source Data	This paper	Mendeley Data: https://doi.org/10.17632/j4kdb59xyf.1
Experimental Models: Cell Lines		
HeLa	ATCC	Cat# CCL-2, RRID:CVCL_0030
HCT-116	ATCC	Cat# CCL-247, RRID:CVCL_0291
HEK293T	ATCC	Cat# CRL-3216, RRID:CVCL_0063
OCI-AML2	Laboratory of Kris Wood	N/A
MEF	Laboratory of Tyler Jacks	N/A
KPR8	Laboratory of Tyler Jacks	N/A
Oligonucleotides		
siBRD2	Thermo Fisher Scientific	Cat# s12071
siBRD3	Thermo Fisher Scientific	Cat# s15545
siBRD4	Thermo Fisher Scientific	Cat# 23902
siHEXIM	Thermo Fisher Scientific	Cat# s20843
siTop2a	Dharmacon	Cat# L-004239-00-0005
siTop2b	Dharmacon	Cat# L-004240-00-0005
siXPF	Dharmacon	Cat# L-019946-00-0005
siXPG	Dharmacon	Cat# L-006626-00-0005
siRNA negative control	Thermo Fisher Scientific	Cat# 4390846
qPCR primer sets	This paper	Source Data File
Recombinant DNA		
pCW57-GFP-2A-MCS	Barger et al., 2019	Addgene #71783, RRID:Addgene_71783
pLenti CMV rtTA3 Blast (w756-1)	Laboratory of Eric Campeau	Addgene #26429, RRID:Addgene_26429
ppyCAG_RNaseH1_WT	Chen et al., 2017	Addgene #111906, RRID:Addgene_111906
ppyCAG_RNaseH1_WKKD	Chen et al., 2017	Addgene #111905, RRID:Addgene_111905
ppyCAG_RNaseH1_D210N	Chen et al., 2017	Addgene #111904, RRID:Addgene_111904
pCW57-mCherry-2A-BRD4 Iso A	This Paper	N/A
pCW57-mCherry-2A-BRD4 Iso C	This Paper	N/A
pCW57-mCherry-2A-BRD4 Iso AdelCTD	This Paper	N/A
pCW57-mCherry-2A-BRD4 Iso CdelET	This Paper	N/A
Software and Algorithms		
CellProfiler-3.1.8	McQuin et al., 2018	https://cellprofiler.org/home
deepTools-3.2.0	Ramírez et al., 2016	https://deeptools.readthedocs.io/en/develop/
IGV-2.7.2	Robinson et al., 2011	http://software.broadinstitute.org/software/igv/

RESOURCE AVAILABILITY

Lead Contact

Further information and requests for resources and reagents should be directed to and will be fulfilled by the Lead Contact, Scott Floyd, M.D., Ph.D. (scott.floyd@duke.edu).

Materials Availability

Plasmids generated in this study have been deposited to Addgene (Cat#s 137720-137723).

Data and Code Availability

The datasets generated during this study are available on the Gene Expression Omnibus (GSE141763). Source data and Cellprofiler pipelines are available is available (Mendeley Data: https://doi.org/10.17632/j4kdb59xyf.1).

EXPERIMENTAL MODEL AND SUBJECT DETAILS

Cell Culture

HeLa (ATCC), HEK293T (ATCC), mouse embryonic fibroblast (MEF), and K-rasV12D-p53 deleted (KPR8) cells were cultured in Dulbecco's modified Eagle's medium (DMEM) (Genesee Scientific) supplemented with 10% fetal bovine serum (FBS) (Summerlin Scientific Products) and 1% penicillin/streptomycin (P/S) (Thermo Fisher Scientific). HCT-116 (Duke Cell Culture Facility-verified) cells were cultured in McCoy's 5A medium (Thermo Fisher Scientific) supplemented with 10% FBS and 1% P/S. OCI-AML2 cells were cultured in Roswell Park Memorial Institute 1640 medium (RPMI) (Thermo Fisher Scientific) supplemented with 10% FBS and 1% P/S. MEF and KPR8 cells were kind gift from Tyler Jacks.

Plasmid Construction

The iBRD4 plasmids were constructed using the pCW57-GFP-2A-MCS backbone (Addgene, 71783), which was a gift from Adam Karpf and previously described (Barger et al., 2019). Gibson assembly was used to insert either mCherry-2A-Flag-BRD4L or BRD4S into the backbone in place of the TurboGFP-P2A-hPGK promoter-PuroR-T2A-rTetR region. The C-terminal domain was deleted from BRD4L using PCR (LΔCTD). The extra-terminal domain was deleted from BRD4S using PCR (SΔET). Sanger sequencing was performed to verify the cloning products.

METHOD DETAILS

Antibodies and stains

The following antibodies were used for western blot (WB), immunofluorescence (IF), or ChIP experiments: BRD4 N terminus (1:1000WB, 1:1000IF, ab128874, Abcam); BRD2 (1:500WB, 5848S, Cell Signaling Technology); BRD3 (1:100WB, ab50818, Abcam); RNAPIIpS2 (1:1000WB, 1:50ChIP, 04-1571, EMD Millipore); γH2AX (1:1000WB, 1:1000IF, 9718S, Cell Signaling Technology); γH2AX (1:50ChIP, ab2893, Abcam); α-Tubulin (1:1000WB, 2144S, Cell Signaling Technology); RPA2pS33 (1:500WB, ab211877, Abcam); cleaved PARP (1:1000WB, 5625, Cell Signaling Technology); BrdU (1:20IF, 347580, BD Biosciences); BrdU (1:80IF, ab6326, Abcam); V5 (1:1000IF, 1:50ChIP, ab9116, Abcam); Total RNAPII (1:000WB, 1:50ChIP, ab817, Abcam); Cleaved Caspase 3 (1:500WB, 9664S, Cell Signaling Technology); SETX (1:500WB, ab220827, Abcam); SRSF1 (1:500WB, 324600, Thermo Fisher Scientific); DHX9 (1:1000WB, PA519542, Thermo Fisher Scientific); HEXIM1 (1:1000WB, ab25388, Abcam); Top2a (1:1000WB, ab52934, Abcam); Top 2b (1:1000, ab72334, Abcam); XPF (1:1000WB, ab76948, Abcam); XPG (1:1000WB, ab224815, Abcam); Goat Anti-Rabbit IgG 800CW (1:6000WB, 926-32211, LI-COR Biosciences); Goat Anti-Mouse IgG 680RD (1:6000WB, 926-68070, LI-COR Biosciences); Goat Anti-Rat IgG 680LT (1:6000, 926-68029, LI-COR Biosciences); Goat Anti-Rabbit IgG Alexa Fluor 647nm (1:500IF, A211245, Life Technologies); Goat Anti-Rabbit IgG Alexa Fluor 555nm (1:500IF, A21428, Invitrogen); Goat Anti-Rabbit IgG Alexa Fluor 488nm (1:500IF, A11008, Life Technologies); Goat Anti-Mouse IgG Alexa Fluor 488 (1:500IF, A11001, Invitrogen); Goat Anti-Rat IgG Alexa Fluor 647 (1:500IF, A21247, Invitrogen).

DAPI (1:2000IF, Thermo Fisher Scientific) was used to stain nuclei. SYBR Gold (1X, Thermo Fisher Scientific) was used to stain single cell electrophoresis (comet) assay. Propidium Iodide (50 μg/mL, VWR) was used to stain nuclei for cell cycle analysis.

Immunofluorescence

Cells were grown on coverslips or in micro-chamber wells (Ibidi) overnight before induction or treatment. When the experiment was completed, cells were washed with ice cold PBS and fixed with 4% paraformaldehyde for 20 minutes at room temperature (RT). After fixation, cells were washed with PBS and then blocked in 5% goat serum and 0.25% Triton-X for 1 hour at RT, rocking. Following blocking, primary antibodies were diluted in the same blocking buffer and incubated at 4°C overnight, rocking. Following incubation with primary antibody, cells were washed three times with PBS and stained with the appropriate secondary antibody diluted and DAPI in blocking buffer at RT for 1 hour, rocking. After incubation with secondary antibody, cells were washed three times with PBS. In the case of cells grown on coverslips, cells were mounted on slides using Prolong Gold (Thermo Fisher Scientific) before

imaging. Cells grown in micro-chamber wells were left in PBS before immediate imaging. Immunofluorescence images were taken either on a Zeiss Axio Observer or EVOS microscope using a 40X objective. Quantification of γH2AX foci was performed using the speckle counting pipeline in CellProfiler (McQuin et al., 2018). All images within a single experiment were fed into the same pipeline and speckles (foci) were counted in an unbiased fashion using the automated program. γH2AX signal is defined as the multiplication of foci count of a nucleus with the mean integrated intensity of the foci within that nucleus.

Western Blotting

Whole cell lysates were prepared with a whole cell lysis buffer (50mM Tris-HCl pH 8.0, 10mM EDTA, 1% SDS) with protease and phosphatase inhibitors (Thermo, 78440) added fresh. Lysates were then sonicated using a QSonica Q700 sonicator for two minutes with an amplitude of 35. After sonication, protein concentrations were determined using BCA reagents (Pierce), compared to protein assay standards (Thermo Fischer Scientific), and absorbance at 562 nm was read using a Spectramax i3x. Equivalent amounts of total protein were resolved by SDS-PAGE gels and transferred to nitrocellulose membranes. Membranes were then blocked with a 1:1 solution of PBS and Odyssey Blocking Buffer (LI-COR Biosciences) at RT for one hour, rocking. Primary antibodies were then diluted in the blocking buffer as described above and incubated with the membranes at 4°C overnight. Membranes were then washed three times with 0.2% Tween-20 in PBS (PBS-T). The appropriate secondary antibodies were also diluted in the blocking buffer and incubated with the membranes at RT for one hour. Membranes were then washed with PBS-T three times and scanned using a LI-COR Odyssey scanner. Quantification and normalization of western blot signal was accomplished with LI-COR software, Image Studio.

Single Cell Electrophoresis (Comet) Assay

Neutral comet assays were performed using the CometAssay Reagent Kit (Trevigen) according to the manufacturer's protocol. Briefly, cells were washed in ice cold PBS, scraped from the plate, mixed with low melt agarose and spread onto supplied microscope slides in the dark. The agarose was gelled at 4°C for 30 minutes before being submerged in the supplied lysis buffer 4°C overnight in the dark. Slides were then incubated with chilled neutral electrophoresis buffer at 4°C for 30 minutes before being subjected to 21V for 45 minutes. Slides were submerged with DNA precipitation solution at RT for 30 minutes and then 70% ethanol at RT for 30 minutes. Slides were then dried and stained with 1X SYBR gold as described above. Comets were imaged on a Zeiss Axio Observer using a 10X objective. Comets were quantified using the comet pipeline from CellProfiler. All images within a single experiment were fed into the same pipeline and comets were quantified in an unbiased fashion using the automated program. Extent Tail moment is defined as Tail DNA % multiplied by the length of the comet tail.

Transfections

For RNA interference, cells were incubated with Thermo Fisher *Silencer*® Select Pre-designed or Dharmacon ON-TARGETplus siRNAs for BRD2 (Thermo, s12071), BRD3 (Thermo, s15545), BRD4 (Thermo, 23902), HEXIM (Thermo, s20843), Top2a (Dharmacon, L-004239-00-0005), Top2b (Dharmacon, L-004240-00-0005), XPF (Dharmacon, L-019946-00-0005), XPG (Dharmacon, L-006626-00-0005), or negative control (Thermo, 4390846). Cells were transfected with Lipofectamine RNAiMAX transfection reagent (Invitrogen) according to the manufacturer's protocol.

For transfection of RNase H1 constructs, cells were transfected with WT RNase H1 (Addgene, 111906), the D210N mutant (Addgene, 111904), or WKKD mutant (Addgene, 111904) which were a gift from Xiang-Dong Fu and previously described (Chen et al., 2017). 750 fmol of plasmid was incubated with a 6:1 ratio of Xtremegene HP transfection reagent at RT for 20 minutes in 1 mL of Opti-mem media. The transfection mixture was then added dropwise to a 10cm dish containing cells at 70% confluence for 24 hours. Cells were then selected with 100 μg/mL hygromycin for 24 hours before fixing (for immunofluorescence experiments) or immediately fixed (for ChIP experiments).

DNA Fiber Analysis

DNA fiber analysis was performed as previously described (Quinet et al., 2017). Briefly, cells were plated at $1x10^5$ cells per well in a 6-well plate and incubated overnight. Cells were then pulsed with the appropriate thymidine analog and treated as shown in Figure 2G. Cells were then washed with PBS and placed on Superfrost Plus Microscope slides and lysed. Following lysis, slides were tilted by raising the edge of the slide 2.2 cm to allow DNA fibers to stretch along the slide and left to dry. DNA was then fixed in 3:1 methanol: acetic acid, dried, and washed in PBS before HCl denaturation of the DNA. The slides were then blocked in 5% BSA before being stained with primary antibodies to detect IdU (mouse anti-BrdU) or CldU (rat anti BrdU). Slides were then stained with the appropriate secondary antibodies before imaging. Images were taken on a Leica SP5 microscope using a 100X objective. ImageJ was used to measure lengths of fibers.

Small Molecule Inhibitors

The BET protein degrader dBET6 was a gift from Nathanael Gray and previously described (Winter et al., 2017). dBET6 was used at a concentration of 100 nM in all experiments except those involving the iBRD4 system, in which it was used at 10 nM. The BET bromodomain inhibitor JQ1 was a gift from James Bradner and previously described (Filippakopoulos et al., 2010). JQ1 was used at a concentration of 500 nM for all experiments. The CDK9 inhibitor DRB (Cayman Chemical Company, 10010302) was used at a concentration of 100 μM for all experiments. The TFIIH inhibitor triptolide (EMD Millipore, 645900) was used at a concentration of 250 nM

(HeLa) or 1 μM (HCT-116). The topoisomerase I inhibitor, camptothecin (Selleck Chemicals), was used at a concentration of 10 μM. The topoisomerase II inhibitor, dexrazoxane (Selleck Chemicals), was used at a concentration of 50 μM. The BET bromodomain inhibitors OTX015 (Selleck Chemicals), ABBV-075 (Selleck Chemicals), ABBV-744 (Selleck Chemicals), and PLX51107 (Selleck Chemicals) where used at 2 μM, 20 nM, 50 nM, and 2 μM, respectively.

EdU Detection

EdU detection was performed using the EdU-Click Chemistry 488 kit (Sigma-Aldrich, BCK-EDU488) according to manufacturer's instructions. In brief, cells were pulsed with 10 μM EdU alongside simultaneous treatment with DMSO or dBET6. Cells were then fixed, washed with PBS, and blocked as described above. Cells were then incubated at RT for 30 minutes in the click chemistry cocktail. Following incubation, cells were washed three times with PBS. After the click chemistry was completed, cells were further process according to the immunofluorescence methods described above.

Flow Cytometry and Cell Cycle Analysis

For cell cycle analysis, cells were trypsinized and washed with ice cold PBS. Cells were then fixed with 70% ethanol at 4°C for 30 minutes. Cells were then washed with PBS twice before being incubated with 100 μg/mL RNase A and 50 μg/mL propidium iodide overnight at 4°C. Cells were then quantified by flow cytometry for DNA content on a BD FACSCanto II machine. For analysis, flow results were entered into the univariate cell cycle modeling in FlowJo for the distribution of cell cycle. Analysis of sub-G_1 populations was performed as previously described (Riccardi and Nicoletti, 2006).

For EdU and γH2AX flow experiments, cells were fixed and stained according to the EdU click chemistry and immunofluorescence methods described above. Cells were then quantified for EdU and γH2AX signal on a BD FACSCanto II machine. FlowJo was then used to generate the figures. Cells that were not pulsed with EdU were used as a negative control for EdU click chemistry. Cells not stained with γH2AX primary antibody were used as a negative control for γH2AX staining.

Chromatin Immunoprecipitation Followed by Next Generation Sequencing (ChIP-seq)

Wild-type HeLa cells (ChIP) or cells transfected with RNase H1 D210N (R-ChIP) were both prepared for qPCR or sequencing using the SimpleChIP® Plus Sonication Chromatin IP Kit according to the manufacturer's instructions. In brief, cells were washed with ice cold PBS and then fixed with 1% formaldehyde in PBS at RT for 13 minutes. The fixation reaction was then halted using a 1X Glycine solution. Cells were then scraped from the plates and pelleted. Cells were then incubated with 1X ChIP sonication cell lysis buffer plus protease inhibitors (PIC) on ice for 10 minutes. Cells were then pelleted and the previous step was repeated. Nuclei were then pelleted and resuspended in ice cold ChIP Sonication Nuclear Lysis buffer with PIC and incubated on ice for 10 minutes. Lysates were then fragmented by sonication with a QSonica Q700 at 4°C for 15 minutes ON-time with a 15 s on, 45 s off program. After sonication, a sample for 2% input was removed. 10 μg of lysates were then incubated with a ChIP grade antibody at 4°C overnight. 30 uL of magnetic beads were then added to the mixture and incubated at 4°C for two hours before going through a series of salt washes. Chromatin was then eluted from the magnetic beads in the elution buffer at 65°C for 30 minutes while vortexing. The supernatant was removed and treated with RNase A followed by Proteinase K. ChIP DNA was then purified using the supplied columns. Library preparation, Next Generation Sequencing, and analysis was performed by GeneWiz to determine the level of ChIP-seq or R-ChIP-seq signal following DMSO or dBET6 treatment for two hours. Log2 ratio normalization to input was accomplished using the bamCompare function of deepTools (Ramírez et al., 2016) with default inputs and viewed using the IGV browser (Robinson et al., 2011).

Chromatin Immunoprecipitation Followed by qPCR (ChIP-qPCR)

DNA for ChIP-qPCR and R-ChIP-qPCR was prepared in the same manner as described for ChIP-seq experiments. Equal volumes of DNA template were subjected to qPCR with qPCR primers designed against the transcription start sites, exons, introns, and transcription termination sites of candidate genes using iTaq Universal SYBR Green Supermix. Samples were normalized to input to determine the relative amounts of ChIP and R-ChIP signal after DMSO or dBET6 treatment for two hours. Primer sequences can be found in the source data file. RNAPII travel ratios were calculated as previously described (Winter et al., 2017).

Graphics

Graphics for this work were generated using biorender.com.

QUANTIFICATION AND STATISTICAL ANALYSIS

Values represent the means ± 1x SEM of independent biological repeats. For immunofluorescence analysis, nuclear intensity, size, and foci were all quantified using CellProfiler pipelines provided in the source data file. Western blot band quantification was done using LI-COR analysis software and independent biological samples were compared using either Student's t test or ANOVA with Tukey's post hoc test as indicated in the figure legends, results and statistics are provided in the source data file. The number of independent biological repeats (n) is provided in the source data file. Asterisks compare to control, unless indicated otherwise in the figure panels, and signify *$p < 0.05$, **$p < 0.01$, ***$p < 0.001$, ****$p < 0.0001$.